Control of Sonic Nozzle Flow With D-Shaped Rib with Sudden Expansion: A Comprehensive CFD Approach

Newaz Md Ashif[1], Syed Ahmed Imran Bellary[2], Vinayak Hanmantasa Khatawate[3], Renita Sharon Monis[4], Shamitha Shetty[5], Sher Afghan Khan[6*], and Shaikh Sarfaraj Jilani[7]

1. Department of Mechanical and Aerospace Engineering, Faculty of Engineering, International Islamic University, Kuala Lumpur, 53100, Malaysia.
2. Department of Robotics and Automation, Zeal College of Engineering and Research, Narhe, SPPU Pune-411041, Maharashtra, India.
3. Department of Mechanical Engineering, SVKM's Dwarkadas J. Sanghvi College of Engineering, Mumbai, India.
4. Department of Mathematics, Shri Madhwa Vadiraja Institute of Technology and Management, Bantakal, Udupi, affiliated to VTU Belgaum, India.
5. Department of Mathematics, Nitte Meenakshi Institute of Technology, Nitte (Deemed to be University), Bangalore 560064, Karnataka, India.
6. Department of Mechanical and Aerospace Engineering, Faculty of Engineering, International Islamic University, Kuala Lumpur, 53100, Malaysia.
7. Department of Robotics and Automation, Zeal College of Engineering and Research, Narhe, SPPU Pune-411041, Maharashtra, India.

Abstract: The development of space shuttles and high-performance military aircraft has made studying turbulent flow in a separated region a vital topic of study. Researchers are also interested in turbulent flow in transonic and supersonic flow. There is considerable relief for the flow when it separates and expands once the area of the larger duct suddenly increases. There are two areas where the shear layer emerges: the separated flow and the main flow. Considerable drag results from the split streamline reattaching to the duct, creating a recirculation zone where the pressure is lower than the surrounding air. Flow from a converging nozzle is suddenly exhausted to a larger diameter. The duct diameter is 22 mm. Base pressure management using a D-shaped rib as a passive control mechanism is the primary focus of this study. The passive control was located at various positions, with a length-to-diameter ratio (L/D) of 0.5, 1, 1.5, 2, and 3. Numerical simulations were conducted for 0.5, 1, and 1.5 mm rib radii. Results indicated that the D-shape rib with a 0.5 mm radius is ineffective, except at nozzle pressure ratios of 4 and 5. The maximum increase in the base pressure is attained for a rib radius of 1.5 mm, and a very moderate rise is obtained for a 1 mm radius. It is observed that the rib locations at L/D = 2 and 3 are ineffective, as the flow becomes attached to the wall around L/D = 1 to 1.5. Hence, one can select the rib radius and height based on the user's requirements.

KeyWords: Base Pressure, L/D ratio, Nozzle Pressure Ratio, Sonic Mach number, Base Drag

1. Introduction

Since the inception of fluid science, turbulence has remained a mystery. Turbulence is a part of the natural and artificial flows around us, and we need to comprehend it. To manage the drag associated with turbulent flows, it is essential to understand the nature of turbulence. Turbulence is sought in some flows when fluids are combined or when an increase

in skin friction drag is needed. However, turbidity is undesirable in engineering flows and should be managed to reduce energy input. In engineering and real-world processes, turbulent drag is associated with significant ecological and financial repercussions. Fossil fuels are applied through a variety of methods. Since the inception of fluid science, turbulence has remained a mystery. Turbulence is a part of the natural and artificial flows around us, and we need to comprehend it. To manage the drag associated with turbulent flows, it is essential to understand turbulence. Turbulence is sought in some flows when fluids are combined or when an increase in skin friction drag is needed. Turbulence is undesirable in engineering flows and should be managed to reduce energy input. In engineering and real-world processes, turbulent drag is associated with significant ecological and financial repercussions. Fossil fuels are applied through a variety of procedures.

The flow fields with sudden expansion are utilized in various fascinating and valuable applications, including parallel diffusers, propulsion systems, and combustion chambers. These flows have been studied because of the necessity of managing such flow fields. Because they produce the desired outcome without requiring additional mechanisms, as active control does, passive control mechanisms have long drawn the attention of scientists due to their simplicity and ease of use. However, the passive control remains with the system as a liability, and this dead weight remains with the system, unlike launch vehicles, which we discard once the propellant is wholly burned. One of the most significant advantages of dynamic control is that it can be utilized as needed.

Numerous applications, including high-speed aircraft, jet engines, rocket motors, rapid entry into a planetary atmosphere, gas pipelines, and commercial uses such as abrasive blasting, utilize the compressible flow effect. While incompressible flow primarily deals with constant density, compressible flow encompasses a variable range of density flows, from subsonic to supersonic.

The analysis of turbulent flow remains an area of ongoing research, driven partly by the development of high-speed missiles, unguided rockets, and supersonic military aircraft.

Flow separation, recirculation, and reattachment are complex characteristics of the axisymmetric expansion flow field. The two primary regions where a shear layer may separate in such a flow field are the recirculation flow region and the primary flow region. The point at which the separating streamline hits the wall is known as the reattachment line. A lot of information regarding sudden expansion issues can be found in the literature. They are, nevertheless, applicable to specific flow and geometrical parameter scenarios. Lowering turbulent drag will help mitigate global warming by reducing CO_2 emissions from the burning of fossil fuels. As a result, efforts should be made to eliminate the near-wall organized structures that significantly contribute to drag production. These near-wall structures can be modified using passive or active control techniques. It is simple to use passive methods, such as splitter plates, riblets, Gurney flaps, bleed, and super-hydrophobic surfaces; however, the drag reduction is relatively small. Active control approaches, on the other hand, can significantly reduce skin friction. Although active control methods can be challenging to implement and require feedback loops, the rewards of exploring different innovative active control methods are alluring.

2. Literature Review

The flow field at sonic and supersonic Mach numbers presents complex challenges due to flow separation, recirculation zones, and base pressure deficits, contributing significantly to

aerodynamic drag. Researchers have extensively explored passive control methods, such as incorporating ribs, cavities, and other geometric modifications, to mitigate these issues and enhance base pressure recovery. Khan et al. [1] conducted experimental investigations using semi-circular ribs in suddenly expanded flows at both sonic and supersonic Mach numbers. Their study compared experimental results with predictions from single-layer and deep neural network models, demonstrating that including ribs effectively increased base pressure and reduced flow separation.

In a complementary study, Khan, Mazlan, and Sulaeman [2] examined the effect of ribs as passive control devices on base pressure at sonic Mach numbers. Their findings indicated that the presence of ribs led to a significant increase in base pressure, attributed to the disruption of the recirculation zone and the promotion of earlier flow reattachment. Further exploring rib geometries, Khan et al. [3] analyzed the impact of various rib configurations in a suddenly expanded flow at sonic Mach numbers. The study revealed that specific rib shapes and placements could optimize base pressure recovery, highlighting the importance of geometric considerations in passive control strategies. Numerical simulations have also played a pivotal role in understanding flow behaviors. Khan, Mazlan, and Ismail [4] performed simulations of suddenly expanded flows from converging nozzles at sonic Mach numbers, providing insights into velocity distributions and base pressure variations. Their work highlighted the importance of nozzle geometry and expansion ratios in shaping flow characteristics.

Advancements in computational fluid dynamics (CFD) have facilitated more comprehensive analyses. Khan et al. [5] conducted a CFD study on base pressure control using quarter ribs in sudden expansion ducts at sonic Mach numbers. The research demonstrated that quarter ribs could effectively manipulate the flow field, enhancing base pressure and reducing drag. Building upon this, Khan et al. [6] explored using semi-circular ribs at critical Mach numbers. Their findings emphasized the effectiveness of these ribs in controlling base pressure, particularly at specific Mach number regimes. A considerable amount of data is available in the literature regarding abruptly expanded flow issues, as discussed by Gao & Liu [7], Li et al. [8], Lu et al. [9], and Yan et al. [10], which outline the procedures governing base flows. Passive controls often involve geometric adjustments to the expanded duct, such as cavities and ribs, and modify the jet control to alter the shear layer's stability characteristics and function as flow control. Passive controls are typically less expensive and easier to build. Cavities, such as base and ventilated cavities, are among the most commonly used flow control technologies for regulating flow in abruptly increased flows, and they can enhance base pressure according to the system's needs. Pandey and Rathakrishnan [3] investigated the flow through an axisymmetric duct with annular cavities spaced at regular intervals. They discovered that adding cavity circulation reduces the oscillatory nature of the flow in the enlarged duct, allowing it to increase smoothly from the low pressure to the ambient pressure at which the jet was discharged. Rathakrishnan et al. [11] expanded the analysis to include multiple aspect ratios. They reported that the cavity in the expanded duct had a considerable impact, with the effect being more substantial for longer ducts than shorter ones.

Pandey and Rathakrishnan [12] conducted similar studies for highly subsonic to supersonic flows. They discovered a supplementary circulation to prevent the flow from oscillating due to cavities. This influence was more noticeable in subsonic than supersonic flow regimes. They also found that the enlarged conduit area ratio has a significant effect on base pressure and flow development. Pathan et al. [13] also produced a similar observation.

Vikramaditya et al. [14] conducted an experimental study to investigate the impact of the base cavity on pressure changes in the base section of a conventional missile system with a

high Mach number of 0.7. The primary objective of the investigation was to identify pressure changes and the main factors that drive them. Because the flow is substantially non-uniform, they discovered that the base pressure variation features varied significantly throughout the azimuthal direction due to model asymmetry. They also found that the introduction of the base cavity results in a long-term improvement in base pressure. Khan et al. [15] investigated the benefits of employing multiple cavities to minimize base drag in compressible subsonic flow. By minimizing base drag, the innumerable holes can regulate the base pressure. They concluded that the longer the duct, the more efficient the control using many cavities. Numerous cavities affect the wall pressure at lower L/D ratios but not at higher L/D ratios.

Similarly, the geometric dimensions of the cavity itself determine the base pressure. Khan et al. [15] also further investigated the effectiveness of the dimple in controlling the base pressure at subsonic expanded flow. The base drag will decrease with an increase in base pressure. At lower L/D, the wall pressure is affected, but at higher L/D, it remains unaffected. In this case, the base pressure is also influenced by the geometric parameters of the cavities. Furthermore, Asadullah et al. [16] investigate the effect of single and multiple holes on base fluxes. They concluded that many cavities had a substantially more significant impact on base flows than single cavities.

Rajendran et al. [17] investigated suddenly expanded duct flows with significantly larger cross-sectional areas. They discovered that when NPR increases, the difference in base pressure reduces progressively. The wall pressure of a constant NPR changes continuously over the length of the duct and reaches ambient pressure when the flow passes the duct outlet. Finally, they concluded that the cavity aspect ratio had a significant influence on the flow field and base pressure. They also developed a low-cost, multi-channel data acquisition system (DAQ) and compared it to commercial DAQ systems. Recent research by Afzal et al. [18] and Afzal et al. [19] on supersonic Mach numbers is based on active control, backed by response surface analysis, k-means clustering, and data backpropagation modeling. The number of input variables for the data analysis was the same for the no-control and control groups. Bashir et al. [20] conducted a numerical investigation of turbulence models emphasizing turbulent intensity at low Reynolds number flows. Their work contributed to the selection of appropriate turbulence models for accurate flow simulations.

Baig et al. [21] explored the control of base flows with micro jets, demonstrating the effectiveness of active control methods in managing base pressure and reducing drag. Rehman and Khan [22] focused on controlling base pressure with micro-jets, providing insights into the design and implementation of active flow control techniques.

Faheem et al. [23] conducted an experimental study on the mean flow characteristics of a supersonic multiple-jet configuration, contributing to an understanding of complex jet interactions in high-speed flows. Sajali et al. [24] performed a numerical investigation of the flow field of a non-circular cylinder, providing data relevant to flow control around bluff bodies. Khan et al. [25] investigated the passive control of base drag in compressible subsonic flow using multiple cavities, emphasizing the effectiveness of cavity configurations in reducing drag.

The following section outlines the methodological aspects related to the computational fluid dynamics of the proposed work.

3. Computational Fluid Dynamics

3.1 Governing Equations

The following hypotheses are taken into consideration:

i. Turbulent flow is considered because of the turbulent viscous dissipation effects.
ii. The fluid's viscosity varies with temperature and is compressible.
iii. At atmospheric pressure, the flow exits the duct.
iv. While scanning the literature, we found that the internal flow k-ε turbulence model is the most suitable, as it yields reasonably good results. Sutherland's three-coefficient viscosity model is expressed as follows:

$$\mu' = \mu'_o \left(\frac{T_a}{T_{a,o}}\right)^{3/2} \frac{T_{a,o}+S'}{T_a+S'} \quad (1)$$

The reference viscosity value in kg/m-s is denoted as μ'_o, where μ' represents the viscosity. T_a denotes static temperature; K represents the temperature of a standard reference, and S' is the temperature-dependent Sutherland constant. Three-dimensional continuity equation for compressible flow:

The equation for mass balance is as follows:

$$\frac{\partial \rho}{\partial t} + \underline{\nabla} \cdot (\rho \underline{V}) = 0 \quad (2)$$

Where the fluid's velocity is denoted by V. The equation for momentum balance is:

$$\frac{\partial}{\partial t}(\rho \underline{V}) + \underline{\nabla} \cdot (\rho \underline{V}\underline{V}) + \underline{\nabla} p = \underline{\nabla} \cdot \left[2\mu (\underline{\nabla V})_o^S\right] + \underline{\nabla} \cdot (\tau_{=Re}) \quad (3)$$

Where $(\underline{\nabla V})_o^S = (\underline{\nabla V})^S - \frac{1}{3}(\underline{\nabla} \cdot \underline{V})\underline{I}, \quad (\underline{\nabla V})^S = \frac{\underline{\nabla V} + \underline{\nabla V}^T}{2}$ and $\tau_{=Re}$ is the turbulent stress tensor.
The formulae for total energy are as follows:

$$\frac{\partial}{\partial t}\left[\rho\left(\frac{1}{2}V^2 + u_{int}\right)\right] + \underline{\nabla}\left[\rho\left(\frac{1}{2}V^2 + u_{int}\right)\underline{V}\right] = \underline{\nabla}\left(\lambda \underline{\nabla} T - p\underline{V} + 2\mu \underline{V} \cdot (\underline{\nabla V})_o^S + \underline{V} \cdot \tau_{=Re}\right) \quad (4)$$

Where u_{int} is the internal energy, and λ is the thermal conductivity. Many internal flow simulations use the k-epsilon turbulence model due to its affordability, resilience, and sufficient accuracy. The Ansys Fluent program incorporates the k-epsilon (ε) turbulence model used in this research. The K-equation allowed us to calculate the turbulent kinetic energy.

$$\frac{\partial}{\partial t}(\rho k) + \underline{\nabla} \cdot (\rho \underline{V} k) = \underline{\nabla} \cdot \left[(\mu + \frac{\mu_t}{\sigma_k})(\underline{\nabla} k)\right] - \rho\varepsilon + M_x \quad (5)$$

The turbulent kinetic energy dissipation rate is denoted by ε, the turbulent Prandtl number is σ-k, and the word Mx is the turbulence generation. Precisely, the dissipation (or (-equation)) is controlled by,

$$\frac{\partial(\rho\varepsilon)}{\partial t} = -\underline{\nabla} \cdot (\rho\varepsilon \vec{V}) + \underline{\nabla} \cdot \left[\left(\mu + \frac{\mu_T}{\sigma_\varepsilon}\right)\nabla\varepsilon\right] - C_1 f_1 \left(\frac{\varepsilon}{k}\right) M - C_2 f_2 \frac{\varepsilon^2}{k} \quad (6)$$

Where $\mu_t = \rho f_\mu C_\mu k^2/\varepsilon$ denotes turbulent viscosity, and the arbitrary constants are denoted as $\overline{C_\mu} = 0.09$, $\overline{C_1} = 1.44$, $\overline{C_2} = 1.92$, $\overline{f_\mu} = 1$, $\sigma_k = 1.0$ and $\sigma_\varepsilon = 1.3$.

4. Finite Volume Method

4.1 Geometry and Modelling

The finite volume technique (FVM) was employed to delve further into this investigation. The CFD simulation utilized the ANSYS FLUENT 2024/R2 software to evaluate the fluid flow through the nozzle. We are examining the impact of the D-shape of the rib using a passive control method. The two orientations of the D-shape rib are shown in Figure 1.

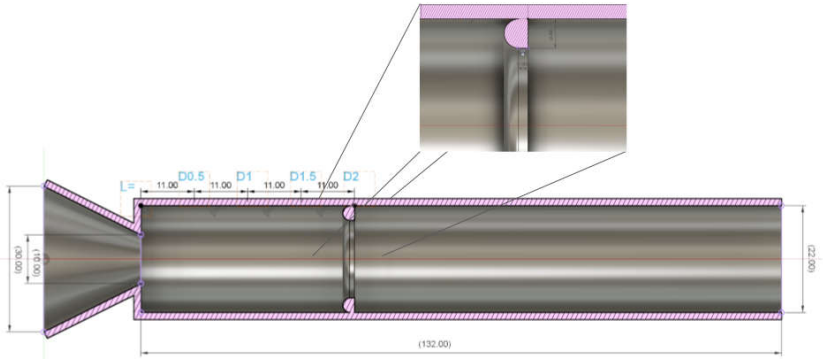

Fig. 1 Rib Orientation

4.2 Meshing and Boundary Conditions

A crucial part of the CFD process is meshing. By choosing the free-face mesh type, the 2D model is of the structured mesh type in this case. Elements were assigned sizes according to the length of each line (edge) when the constructed structured mesh type was used. The lines were utilized to apply the element size, and elements with identical forms were created using face meshing. The mesh independence check is done. Figure 2 below shows the mesh's element type and size tested during the mesh independence check. Mesh independence test for duct 18 mm – without rib (L/D = 6). Different element sizes and their properties are based on the same geometry model.

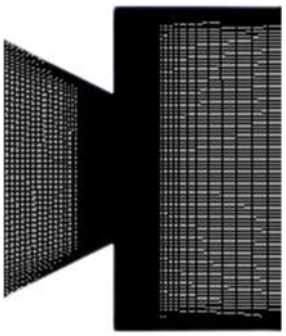

Close view

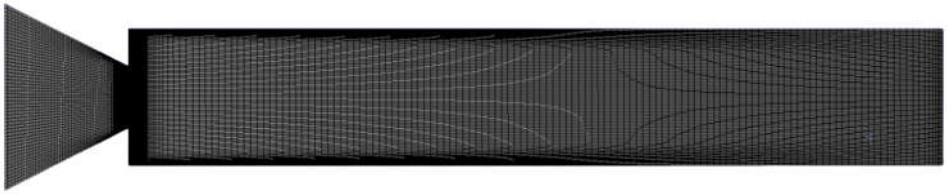

(a)

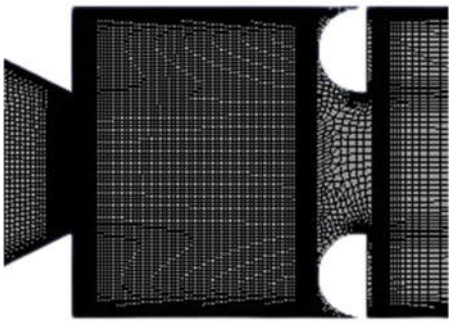

Enlarged view

(b)

Fig.2. Mesh model (a) without control, (b) with control

4.3 Assumptions and Fluid Properties

Assumptions are made to replicate the flow activities in the precise physical environment. Appropriate mathematical and numerical models are selected to simplify the governing equations.

To solve the governing equations simultaneously, numerical modeling requires selecting the appropriate mathematical models, including the governing equations, boundary conditions, mesh quality, and numerical method. Despite its limitations in accurately representing physical phenomena, the computational method has been trusted for decades and offers sufficient insight into flow behavior. As a result, this calls for careful consideration of elements that closely resemble the flow behavior. This study pinpoints the presumptions that jeopardize the precise physical state. The following are the assumptions and characteristics covered in this study:

i. The flow is assumed to be a steady 2D flow because the geometry is symmetric. Hence, the assumption that the flow is 2-D is justified.
ii. The density of the air is variable as the flow is compressible. The inlet pressure is the gauge pressure at that Mach number and NPR, and at the outlet of the duct, the gauge pressure is zero.
iii. Turbulent flow significantly impacts turbulent viscous dissipation at a given flow velocity, so it is considered.
iv. The viscosity of the fluid is dependent on temperature.
v. At standard atmospheric pressure, the flows leave the duct. At normal ambient pressure, they do not.

Since the flow via the nozzle is considered turbulent, the compressible flow field is represented by the k-epsilon standard model. The subsequent equations most appropriately characterize the turbulent flow.

4.4 Validation of Experimental Model

The ANSYS Workbench program utilized fluid flow (Fluent) analytical techniques throughout the computational fluid dynamics (CFD) procedure. The model was generated via a Design Modeler. Figure 3 depicts a converging nozzle that abruptly widens into a duct with five ribs. Rathakrishnan [25] experimental setup, the dimensions of the convergent-divergent nozzle with a suddenly expanded duct are as stated below.

Table 1
The geometries of the validation model

Parameters	Dimensions
Nozzle inlet diameter	30 mm
Nozzle outlet diameter	10 mm
Duct diameter	22 mm
Duct length	Varies from 1D to 6D
Converging length	20 mm
Rib width	3 mm
Rib height	Varies from 1mm to 3mm

Figure 3 illustrates the base pressure ratio data from current and earlier studies [25]. The experimental values were denoted by dotted lines, while the simulation results obtained using ANSYS Fluent were represented by straight lines. The present numerical analysis exhibited a percentage discrepancy of less than 10% compared to the previous experimental study. Consequently, the current work met the criteria for acceptability. The curves exhibited a consistent pattern, with each point closely following the next. As a result, based on the table and graph described before, the validation of the current work was successful.

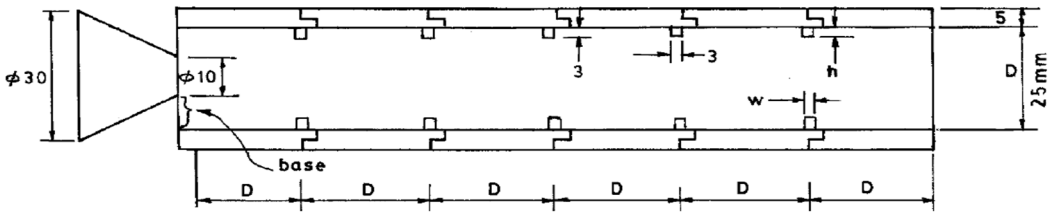

Fig. 3. Duct with five ribs used in an experimental study [26]

According to Rathakrishnan [26], the prior work was performed at aspect ratios of 3:3, 3:2, and 3:1; an area ratio of 6.25; L/D ranging from 1 to 6; pressure ratios of 1.141, 1.295, 1.550, 1.707, and 2.458; and nozzle exit Mach numbers of 0.44, 0.62, 0.82, 0.91, and 1.0. However, in a prior publication by Rathakrishnan [25], the result from Figure 4 with NPR (P_{01}/P_a) of 2.458 and models with control in the form of ribs with aspect ratios of 3:2 and 3:3 was chosen for comparison with the current work. The simulation is supported by Rathakrishnan's [26] experimental work, which used five ribs positioned at equidistant intervals in the duct, as illustrated in Figure 4. The results of base pressure fluctuation with NPR of 2.458 and L/D ranging from 2 to 6 are obtained. The study is repeated to validate the numerical results of a model with control over different rib aspect ratios [26].

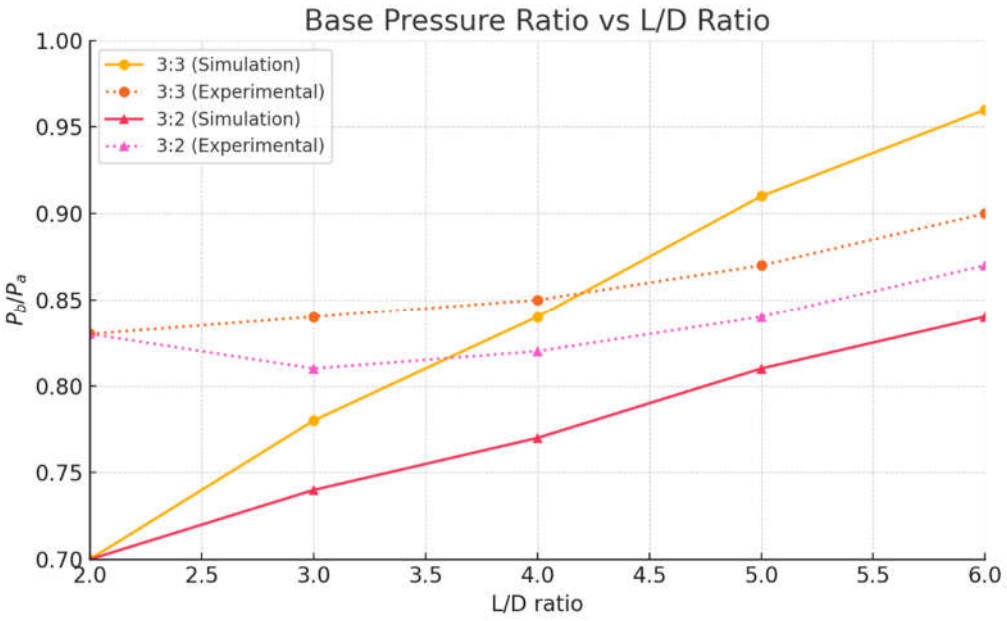

Fig. 4. Validation of previous work by Rathakrishnan [26]

4.5 Mesh Independence Study

Table 2 presents data from a mesh independence study, a crucial step in computational simulations that ensures the results remain consistent regardless of the mesh refinement level. The element sizes range from coarse to fine, with corresponding node and element counts for each mesh configuration. As the mesh becomes finer, the number of nodes and elements increases significantly, from 1,284 nodes and 1,145 elements in the coarsest mesh to 1,354,262 nodes and 1,351,303 elements in the finest mesh. This study aims to determine the optimal mesh size for accurate simulations without unnecessary computational expense. The table shows a notable increase in nodes and elements as the mesh is refined. The coarsest mesh has relatively few nodes and elements, resulting in a lower computational cost but potentially lower accuracy. Conversely, the finest mesh offers the highest resolution at the expense of significant computational resources. The medium and fine meshes provide intermediate levels of refinement, offering a balance between accuracy and efficiency.

Table 2
Mesh independence study

Element size	Coarsest	Coarse	Medium 1	Medium 2	Fine	Finer	Finest
Nodes	2703	5573	18053	35486	264734	762769	3885169
Elements	2500	5286	17577	34838	263101	760026	3879157

Based on the trends in node and element numbers, the finest mesh will likely produce the most accurate results (Figure 5). However, continuing to refine the mesh beyond a certain point may offer diminishing returns in terms of accuracy while significantly increasing computational time. A critical assessment of this table would suggest that the "Fine" or "Finer" mesh configurations may represent the best balance between accuracy and computational efficiency. These configurations substantially increase the number of nodes and elements compared to the medium meshes without reaching the computational expense of the finest mesh. If the simulation results do not change significantly between the fine and

finest meshes, further refinement of the finest mesh is unnecessary, as it would only increase computational time without added benefit. Thus, the fine or finer mesh sizes are likely the best choices for further simulation.

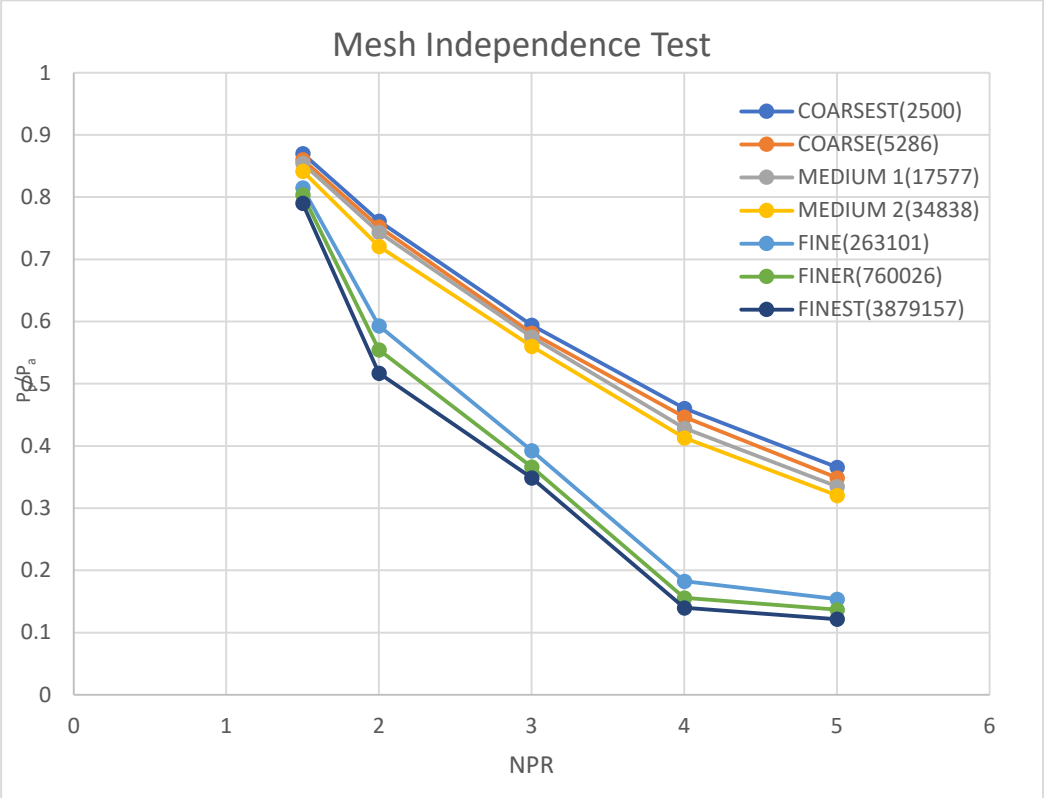

Fig. 5: Results of mesh check

5. Results and Discussions

Before examining the findings, it would be helpful to understand the mechanics underlying the sudden increase in relief to the flow. Figure 6(a) illustrates how the boundary layer at the nozzle exit would form a free shear layer for subsonic flows and meet the expanded duct wall downstream.

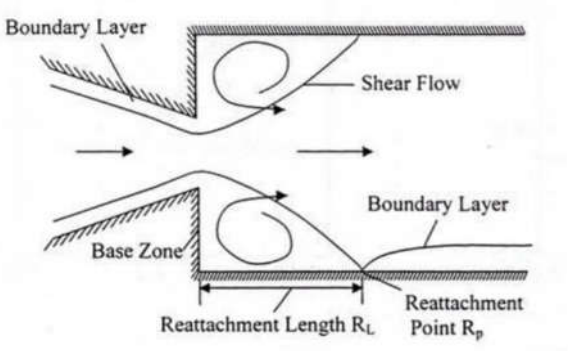

Fig. 6(a) Sudden Expansion Flow Field

The reattachment point is the location where the flow attaches. Reattachment length is the distance between the base and the point of reattachment. One or more vortices will be positioned between the base, the reattachment point, and the edge of the free shear layer. The first, strong vortex near the base is called the primary vortex. That moves fluid from the base to the main flow on the other side of the free shear layer edge. There is low pressure at the base due to this pumping motion. The pumping, however, also becomes periodic since vortex shedding is a periodic event. The base pressure varies as a result of this. Nonetheless, it was found that the base pressure variations were often minimal and could be expressed as a mean value. Oscillatory flow occurs throughout the duct due to the periodicity of the vortex motion. There are several flow and geometrical parameter combinations where the oscillations can get terrible. To adjust the primary vortex strength, the reattachment and the flow Mach number significantly impact the suction at the base and the flow oscillations in the duct.

5.1 Base Control with Orientation 1

Fig. 6(b) shows the arrangement of the nozzle with the enlarged duct and the passive control in the form of a D-shape rib. The section following the base pressure results for D-shape rib orientation one, when the curved part of the rib faces the base recirculation region, will show later results for orientation two, where the straight part of the rib will face flow impinging on the straight part of the D-shape rib. Non-dimensional base pressure results are represented for various rib locations and duct sizes as a function of the nozzle pressure ratio.

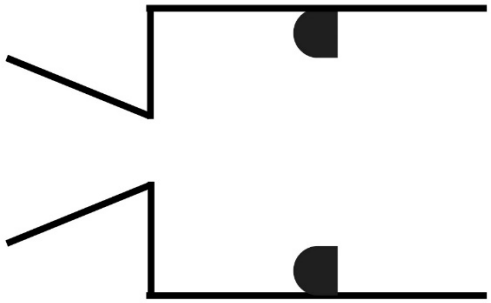

Fig. 6(b). Nozzle and duct assembly with D-shape Rib for orientation 1

5.1.1 Base Pressure Results for Rib Location at L/D = 0.5

In this section, we focus on the impact of passive control through a D-shaped rib with varying radii, ranging from 1 mm to 3 mm, and duct lengths from 1D to 6D. The resulting base pressure is shown in Figs. ((a) to (f)). For rib orientation, the curved part of the rib is oriented to face the shear layer exiting from the nozzle.

Fig. 7(a) presents the outcomes of this study when the rib is placed at L/D = 0.5 for various NPRs. The figure shows that the base pressure is declining in the absence of the rib despite the nozzle being highly under-expanded. That may be due to the considerable relief available to the shear layer as it exits the converging nozzle. In this sudden expansion of the shear layer, the flow reattaches to the duct wall beyond the optimum location. Resulting in a considerable reattachment length, and hence, the declining trend continues despite the nozzle flowing under the influence of a favorable pressure gradient. It is observed that a rib radius of 0.5 mm results in a marginal decline until NPR = 4, after which the declining trend reverses. However, for a rib of radius 3 mm right from NPR = 1.5, there is a progressive rise

in the base pressure; its value is slightly more than the ambient pressure initially, and at the highest value of NPR = 5, the base pressure ratio becomes three.

Meanwhile, for a rib radius of 1 mm initially, until NPR = 2.5, there is a decline in the base pressure. Later, there is a linear increase in the base pressure, with a base pressure ratio of approximately 1.2. The physics behind the flow may be that the location of the rib is very close to the nozzle exit, and the shear layer has not yet separated and stabilized. Hence, we need to examine the base pressure values at the rib location of L/D = 1 and beyond, as the reattachment point is expected to be around L/D = 1 to 1.5.

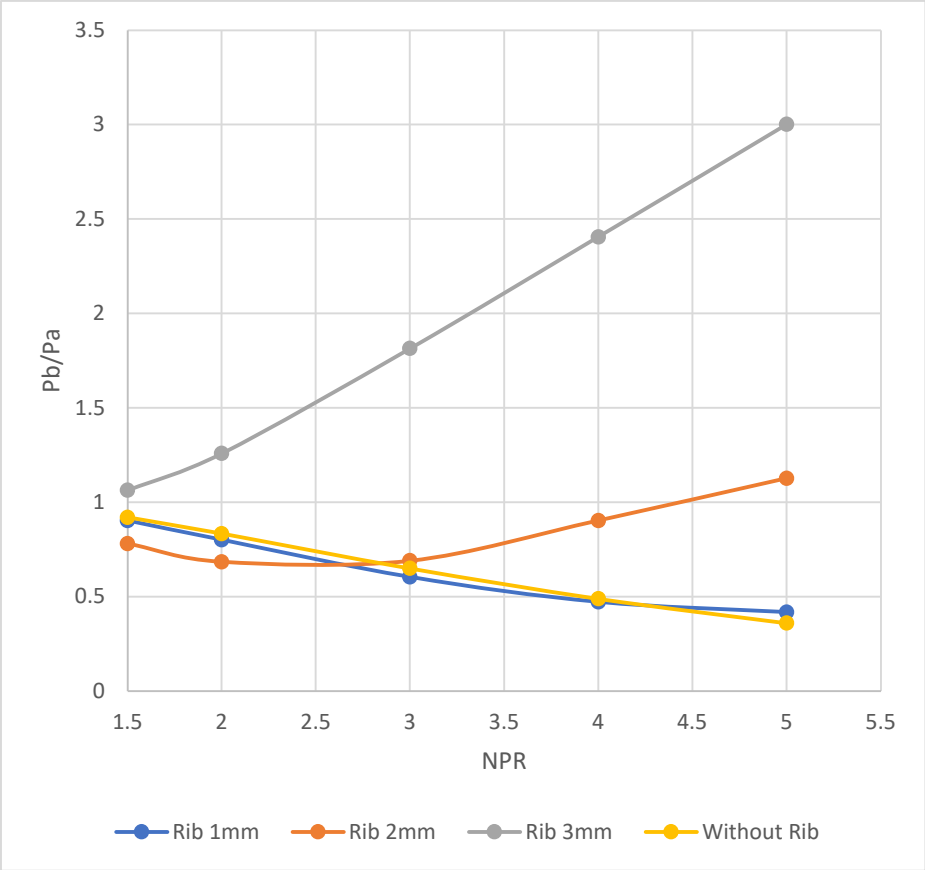

(a) L/D = 1

Similar results are observed for duct lengths of 2, 3, 4, 5, and 6 times the diameter. There is a marginal effect of the duct length on the base pressure, but it still does not reveal a definite trend, as the shear layer continues to expand.

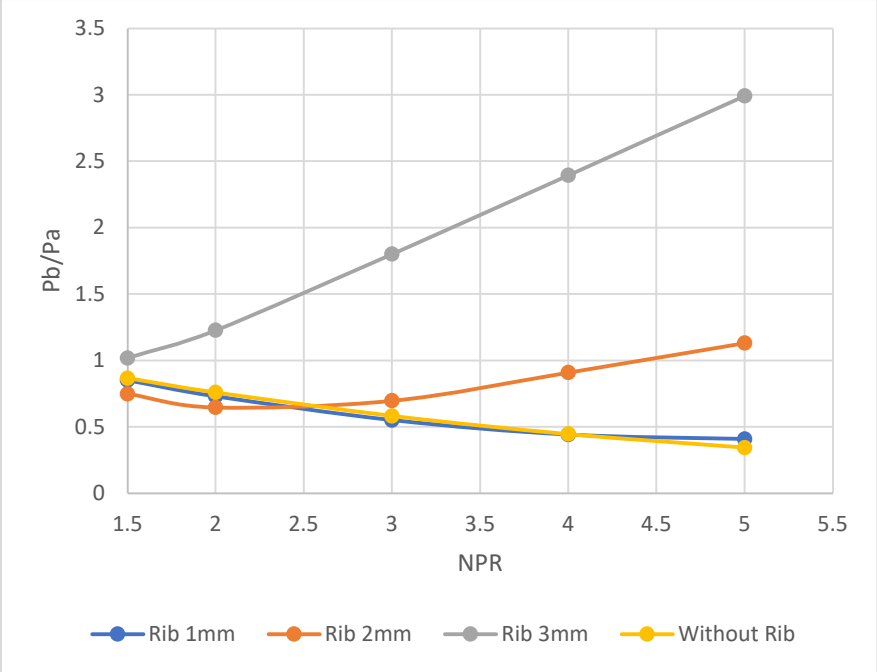
3.5
3
2.5
2
1.5
1
0.5
0
Pb/Pa
1.5
2
2.5
3
3.5
4
4.5
5
5.5
NPR
Rib 1mm
Rib 2mm
Rib 3mm
Without Rib

(b) L/D = 2

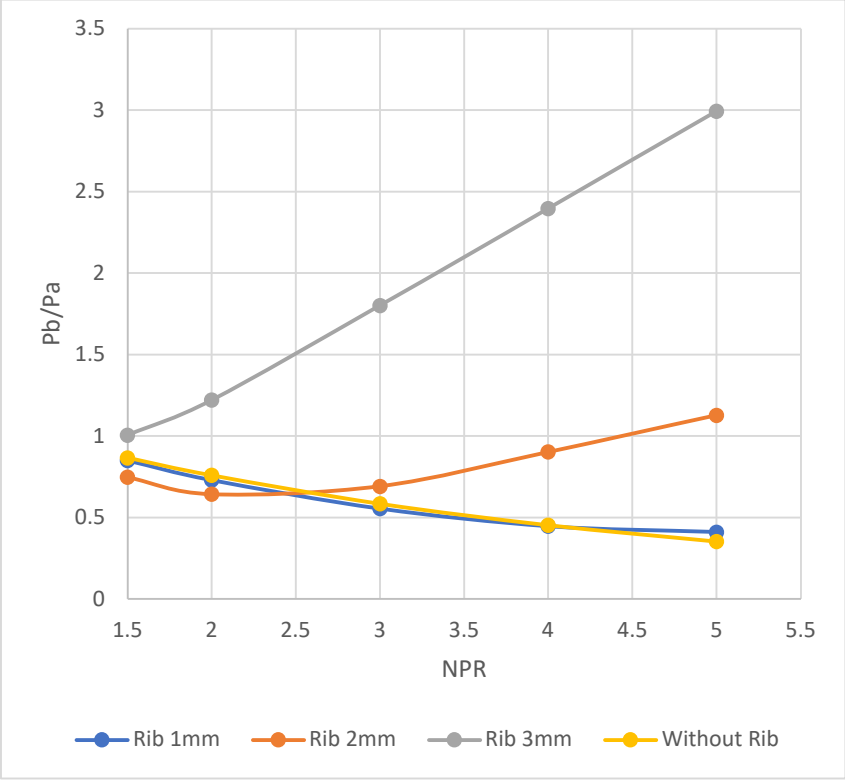
3.5
3
2.5
2
1.5
1
0.5
0
Pb/Pa
1.5
2
2.5
3
3.5
4
4.5
5
5.5
NPR
Rib 1mm
Rib 2mm
Rib 3mm
Without Rib

(c) L/D = 3

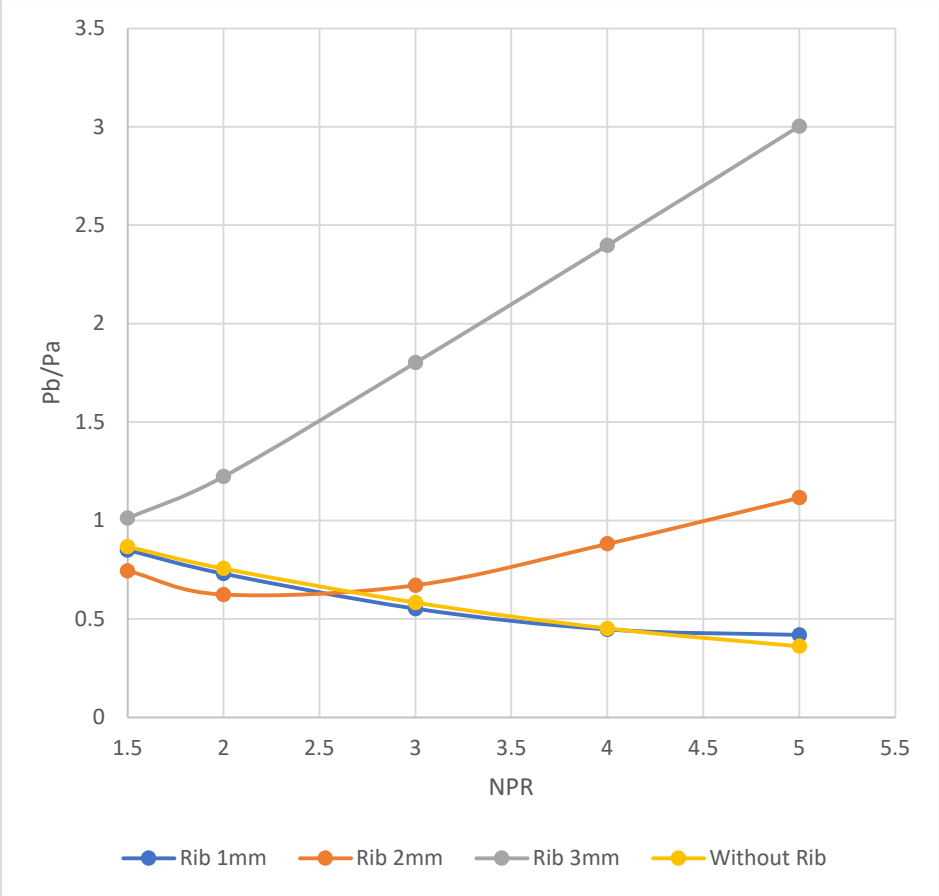
3.5
3
2.5
2
1.5
1
0.5
0
Pb/Pa
1.5
2
2.5
3
3.5
4
4.5
5
5.5
NPR
Rib 1mm
Rib 2mm
Rib 3mm
Without Rib

(d) L/D = 4

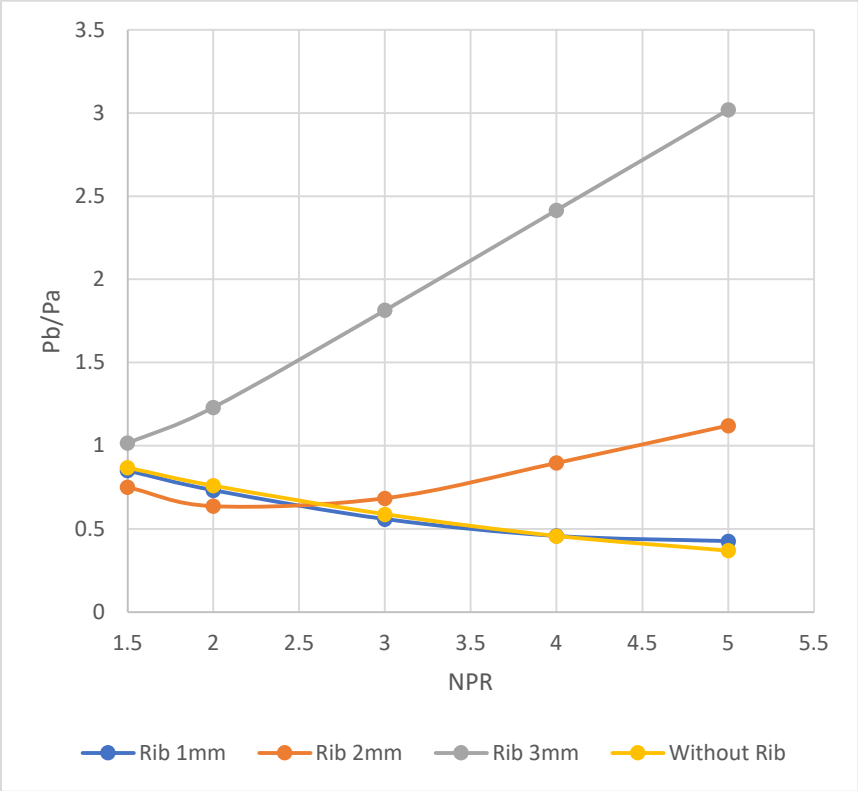
3.5
3
2.5
2
1.5
1
0.5
0
Pb/Pa
1.5
2
2.5
3
3.5
4
4.5
5
5.5
NPR
Rib 1mm
Rib 2mm
Rib 3mm
Without Rib

(e) L/D = 5

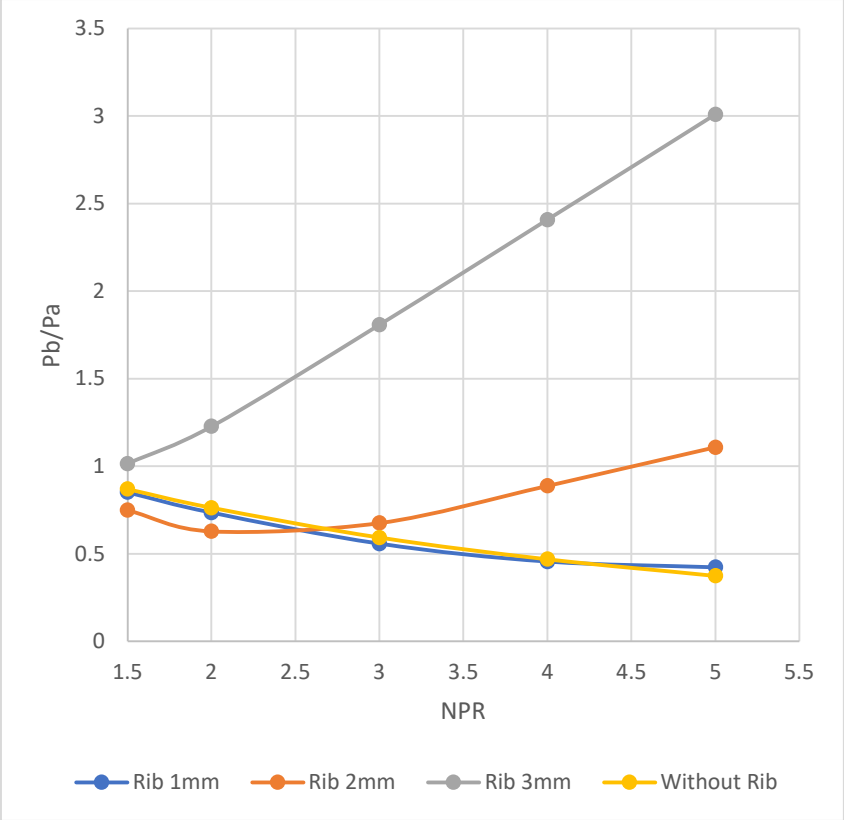

(f) L/D = 6

Fig. 7. Base Pressure Vs. NPR for numerous Duct segments

5.1.2 Base Pressure Results for Rib Location at L/D = 1.0

When the rib is placed at L/D = 1, the findings of this study are shown in Figures 8(a) to (e) for Duct sizes L/D = 2 to 6 for various levels of expansions. Fig. 8(a) shows the outcomes of this study for a duct length of L/D = 2. The figure shows a significant difference in the base pressure ratio for rib radii of 1 mm and 1.5 mm, with a considerable rise in the base pressure ratio for both rib radii. As seen in the previous case, a 0.5 mm radius is not helpful, but there is some improvement compared to the earlier case.

Similar results are observed for other duct lengths; however, the variation in duct length does not significantly impact the base pressure values. The physics of the phenomena may be that the flow is not fully developed, and secondary vortices start interacting with the wall and the dividing streamlines. From the results, it is also evident that the duct size and ambient pressure have an effect, as at this location, the rib has blocked the flow entirely, and hence, the backpressure has no role in modifying the base pressure values. For a 1 mm radius, the decrease in the base pressure seen in the previous case is also absent here. There is a declining trend in the base pressure when the rib is located at L/D = 1 and its radius is 1 mm. This pattern may be due to the location of the rib, which seems to be in this neighborhood of the reattachment point.

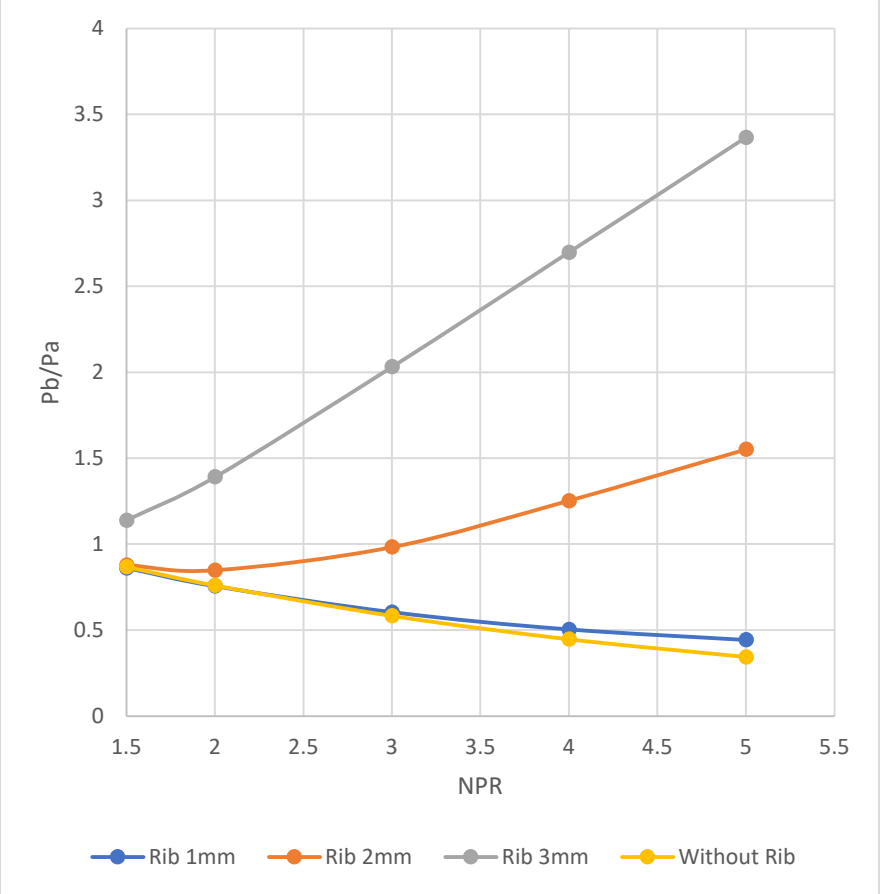
4
3.5
3
2.5
2
1.5
1
0.5
0
Pb/Pa
1.5
2
2.5
3
3.5
4
4.5
5
5.5
NPR
Rib 1mm
Rib 2mm
Rib 3mm
Without Rib

(a) L/D = 2

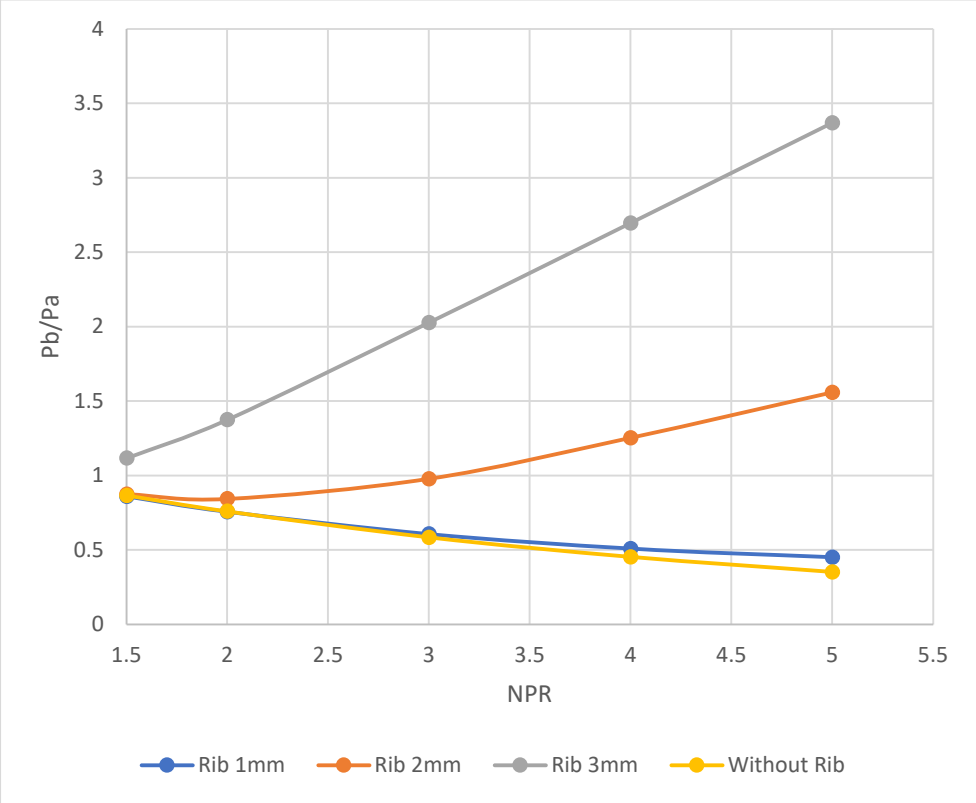
4
3.5
3
2.5
2
1.5
1
0.5
0
Pb/Pa
1.5
2
2.5
3
3.5
4
4.5
5
5.5
NPR
Rib 1mm
Rib 2mm
Rib 3mm
Without Rib

(b) L/D = 3

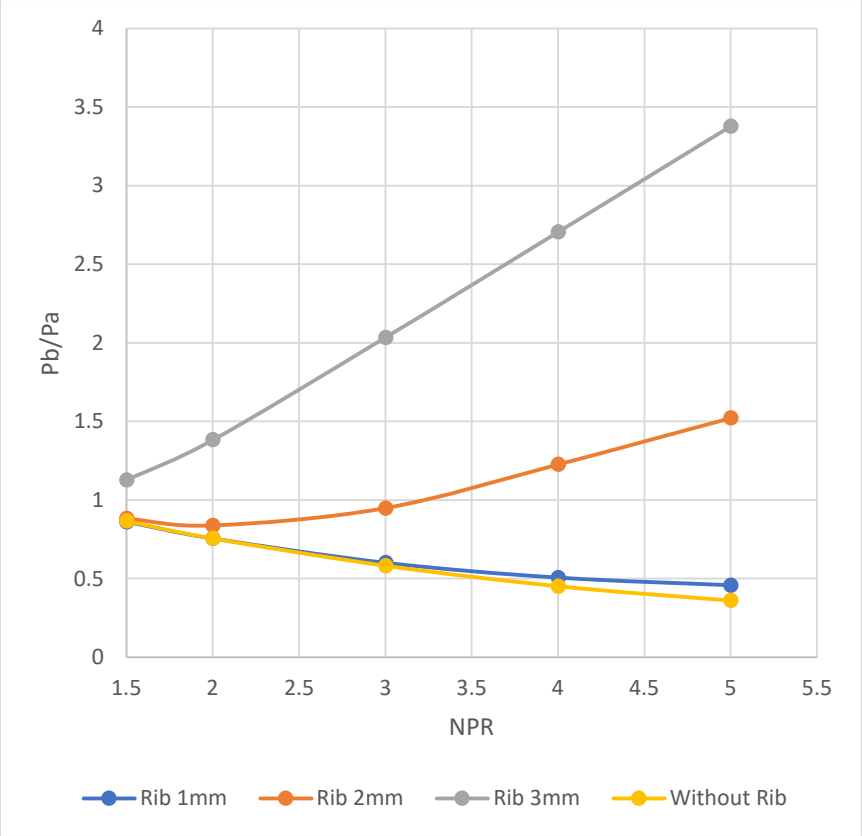
4
3.5
3
2.5
2
1.5
1
0.5
0
Pb/Pa
1.5
2
2.5
3
3.5
4
4.5
5
5.5
NPR
Rib 1mm
Rib 2mm
Rib 3mm
Without Rib

(c) L/D = 4

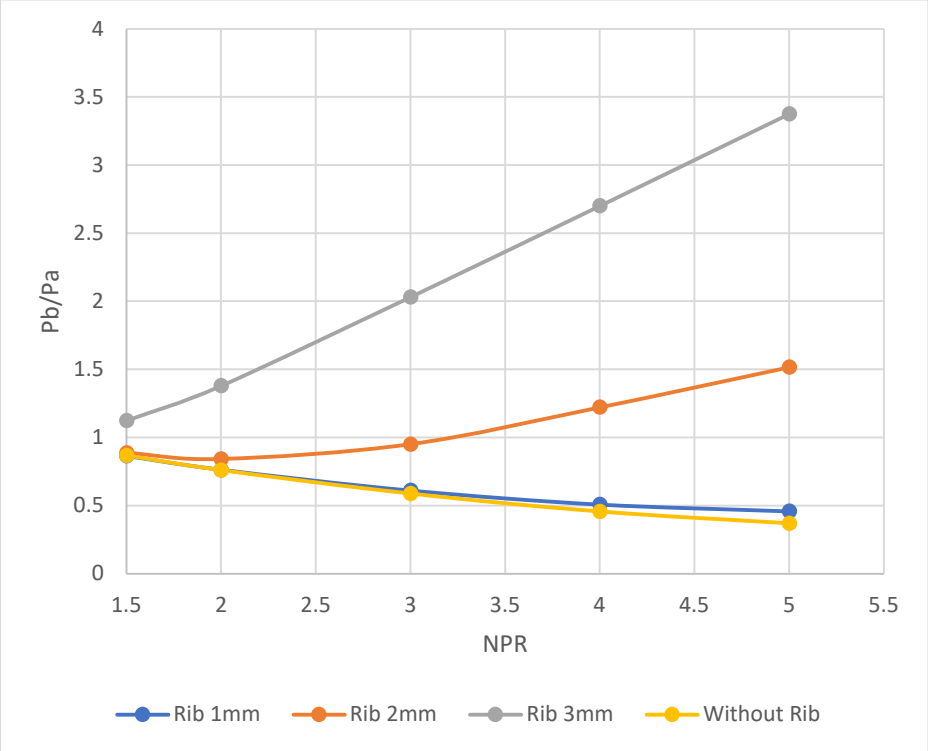
4
3.5
3
2.5
2
1.5
1
0.5
0
Pb/Pa
1.5
2
2.5
3
3.5
4
4.5
5
5.5
NPR
Rib 1mm
Rib 2mm
Rib 3mm
Without Rib

(d) L/D = 5

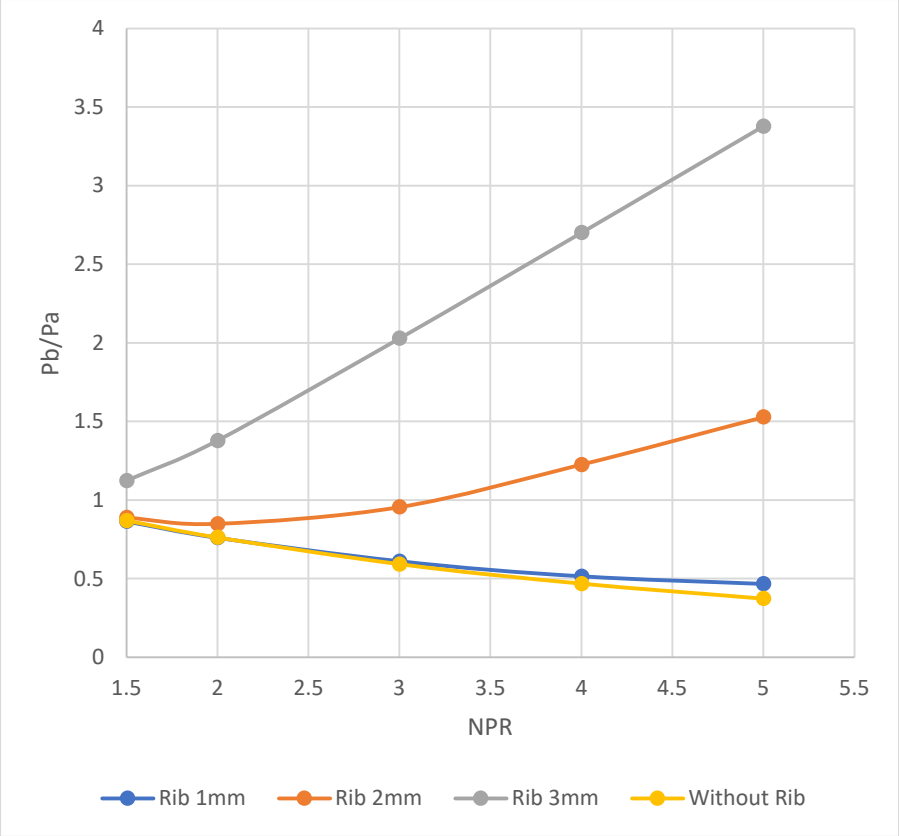

(e) L/D = 6

Fig. 8. Base Pressure Vs. NPR for numerous Duct segments

5.1.2 Base Pressure Results for Rib Location at L/D = 1.5

When the rib is further shifted downstream and placed at L/D = 1.5, the base pressure results for these locations are shown in Figures 9(a) to (e) for NPRs ranging from 1.5 to 5 and duct sizes from L = 2D to 6D. The figure indicates that the shift in the rib location has marginally increased the base pressure for 1.5 mm and 1 mm radii. All other conditions are similar, except that the rib has been shifted toward the downstream. This increase is due to the interaction between the secondary vortices and the dividing streamline that hits the duct wall. Therefore, there will be a considerable change in the pressure once the rib is present. Later, any change in the duct sizes will have a marginal impact on the duct flow field. Moreover, there will be no change in the flow field, as the flow has already become attached to the wall, which will prevent any impact on the ambient pressure and duct size. There is a marginal increase in the base pressure for rib radius 0.5 mm, and control efficiency has marginally improved. Additionally, it is observed that there is a slight change in the base pressure for radii of 1 mm and 1.5 mm over a considerable duct length, specifically L/D = 4 to 6. These changes are attributed to the absence of the influence of duct sizes and back pressure present for L/D = 2 and 3.

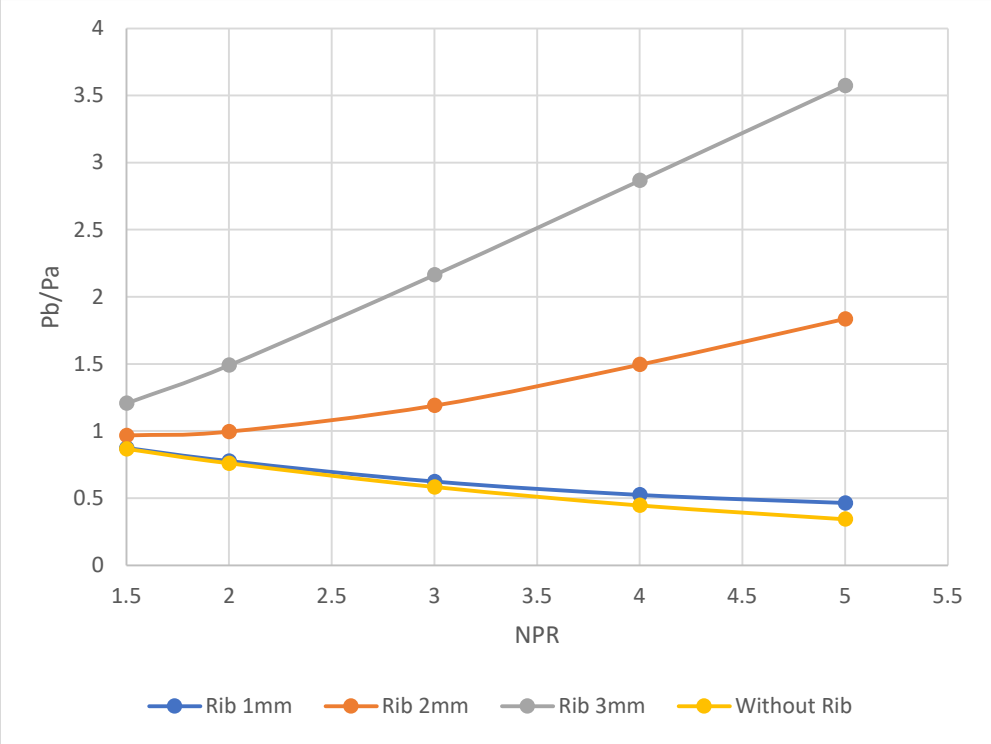
Pb/Pa
NPR
Rib 1mm
Rib 2mm
Rib 3mm
Without Rib

(a) L/D = 2

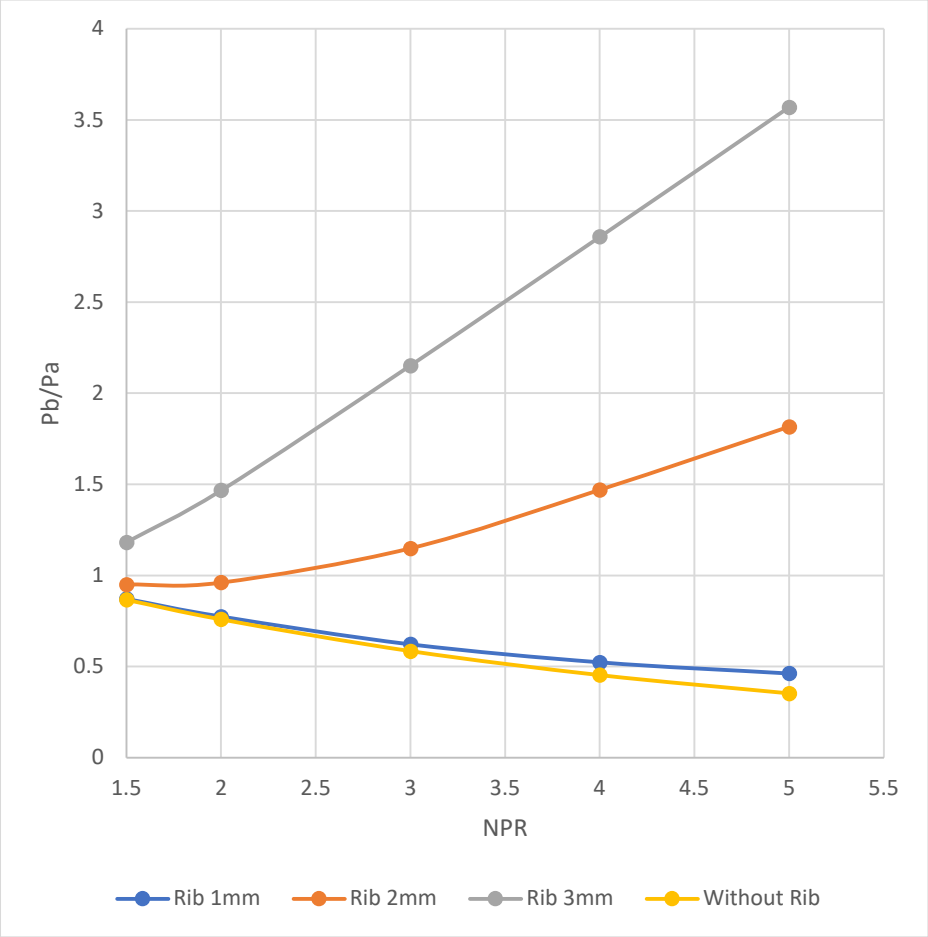
Pb/Pa
NPR
Rib 1mm
Rib 2mm
Rib 3mm
Without Rib

(b) L/D = 3

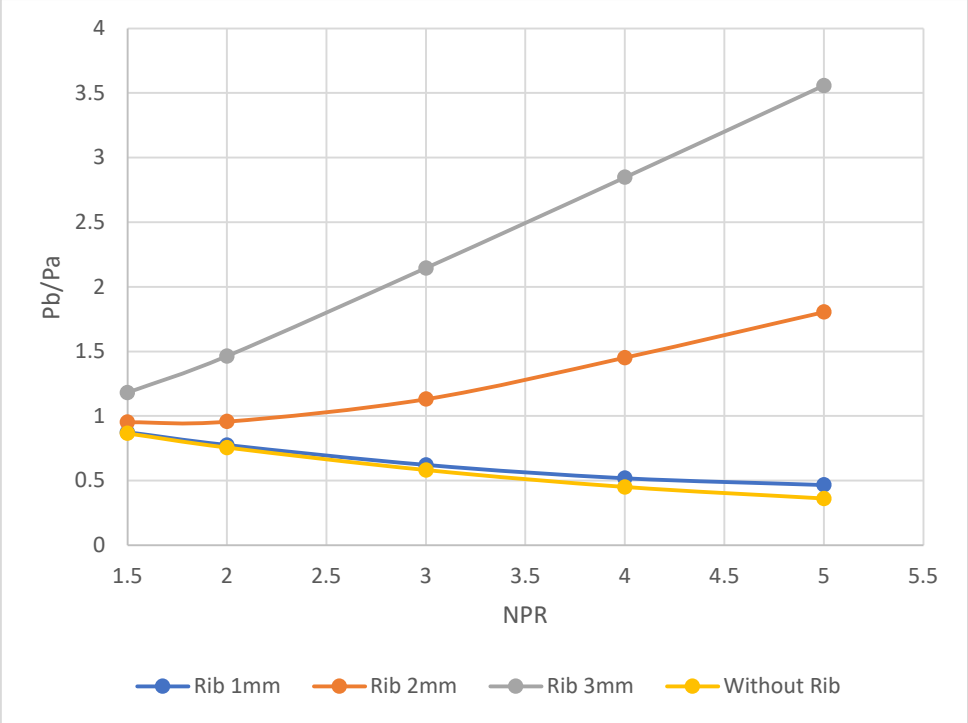
4
3.5
3
2.5
2
1.5
1
0.5
0
Pb/Pa
1.5
2
2.5
3
3.5
4
4.5
5
5.5
NPR
Rib 1mm
Rib 2mm
Rib 3mm
Without Rib

(c) L/D = 4

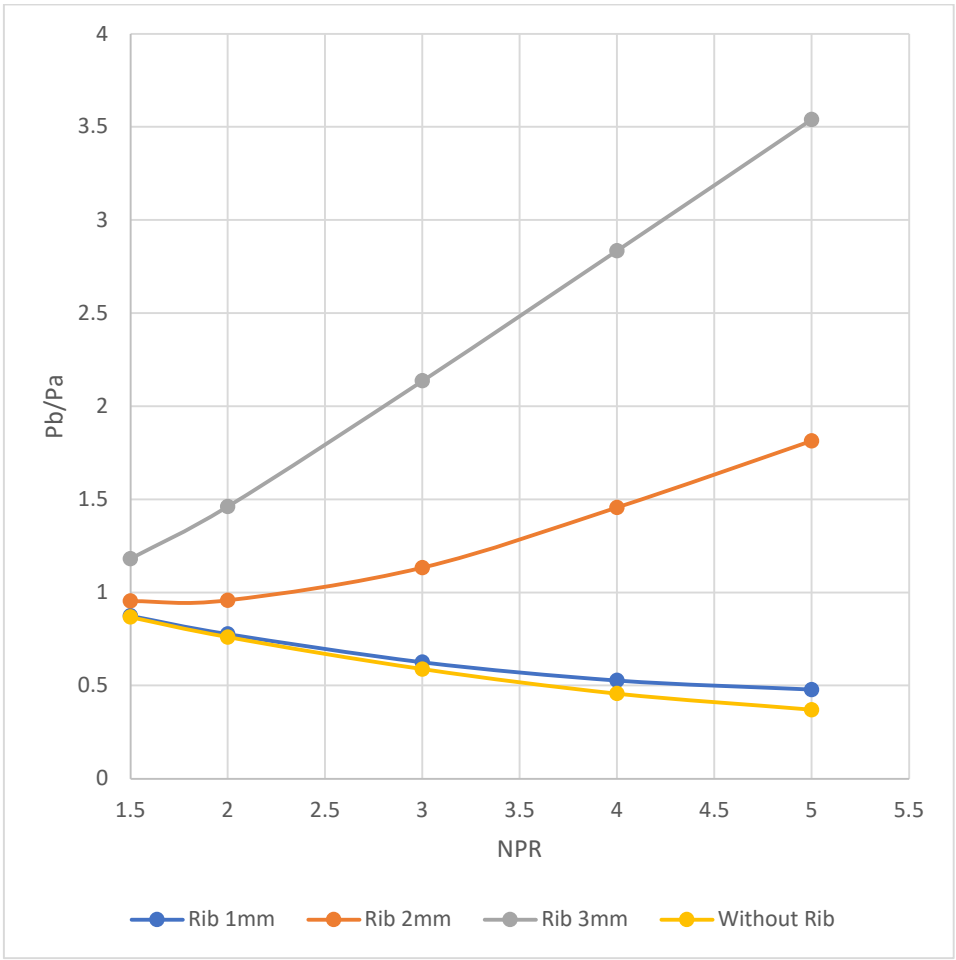
4
3.5
3
2.5
2
1.5
1
0.5
0
Pb/Pa
1.5
2
2.5
3
3.5
4
4.5
5
5.5
NPR
Rib 1mm
Rib 2mm
Rib 3mm
Without Rib

(d) L/D = 5

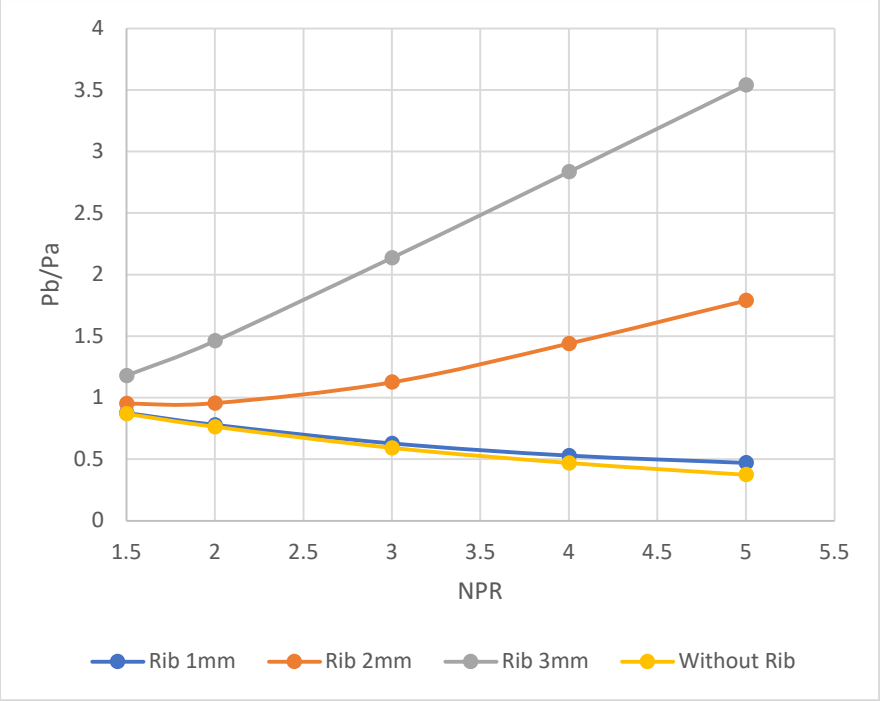

(e) L/D = 6

Fig. 9. Base Pressure Vs. NPR for numerous Duct segments

5.1.4 Base Pressure Results for Rib Location at L/D = 2.0

Base pressure results for rib placement at L/D = 2 are shown in Figures 10 (a) to (d). As discussed earlier, once the flow is attached, the duct size is 22 mm, and the reattachment length seems to be around L/D = 1 to 1.5. Figure 10 (a) shows a slight increase in the pressure values for rib radii of 1 mm and 1.5 mm. However, a 0.5 mm rib radius remains marginally effective for larger NPRs, specifically for NPR values of 3 and above. These results reiterate that there is a threshold value of rib location and size, which results in the maximum gain in base pressure, and these values occur when the rib radii are 1 mm and 1.5 mm, and the rib is located at L/D = 1 or 1.5. Any further shift in the rib location results in a marginal increase in the base pressure for the two most prominent values of the ribs. Therefore, we can conclude that the optimum location of the rib seems to be either L/D = 1 or L/D = 1.5. When the ribs are placed at L/D = 2 and L/D = 3, they are inefficient in regulating the base pressure.

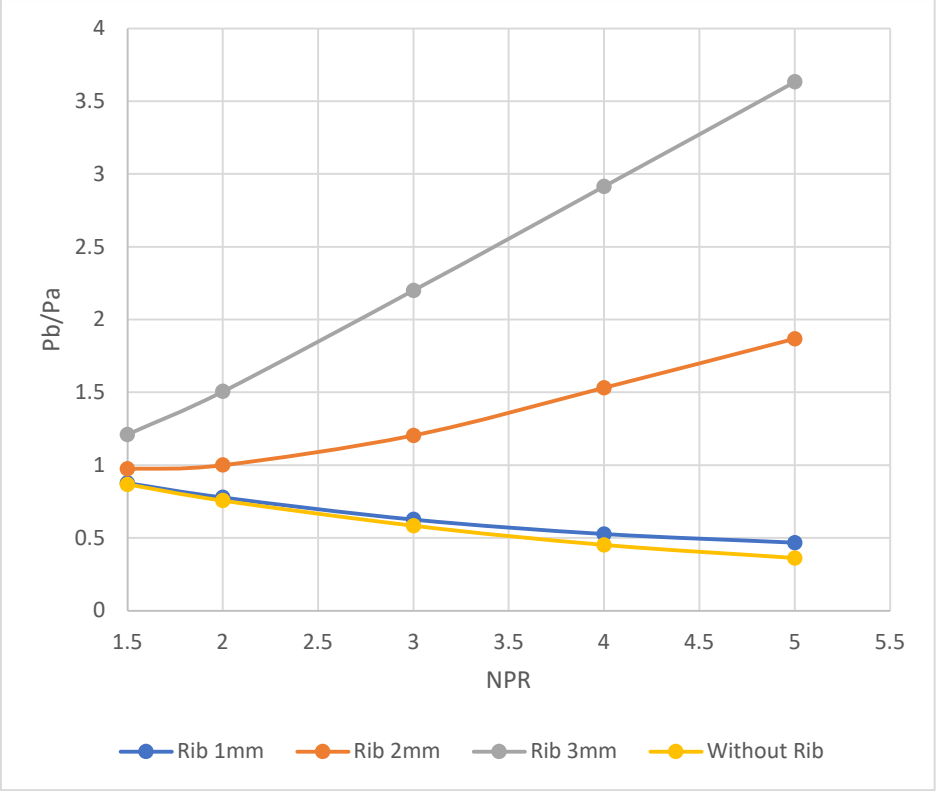
4
3.5
3
2.5
2
1.5
1
0.5
0
Pb/Pa
1.5
2
2.5
3
3.5
4
4.5
5
5.5
NPR
Rib 1mm
Rib 2mm
Rib 3mm
Without Rib

(a) L/D = 3

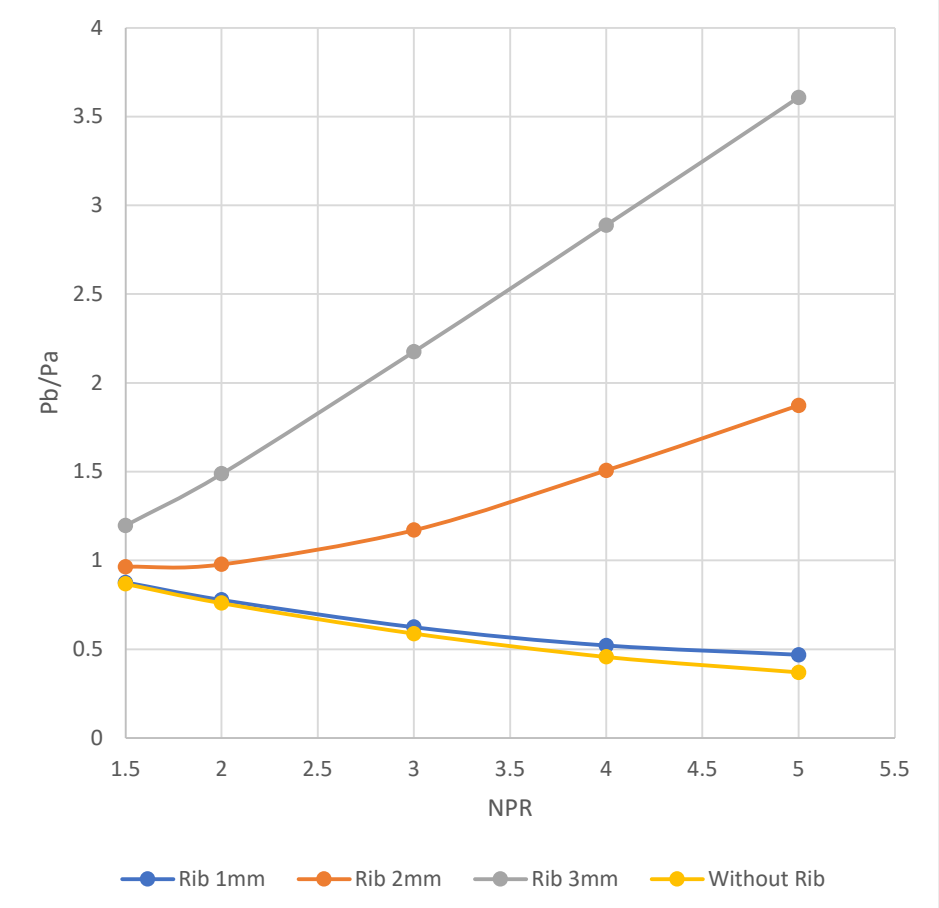
4
3.5
3
2.5
2
1.5
1
0.5
0
Pb/Pa
1.5
2
2.5
3
3.5
4
4.5
5
5.5
NPR
Rib 1mm
Rib 2mm
Rib 3mm
Without Rib

(b) L/D = 4

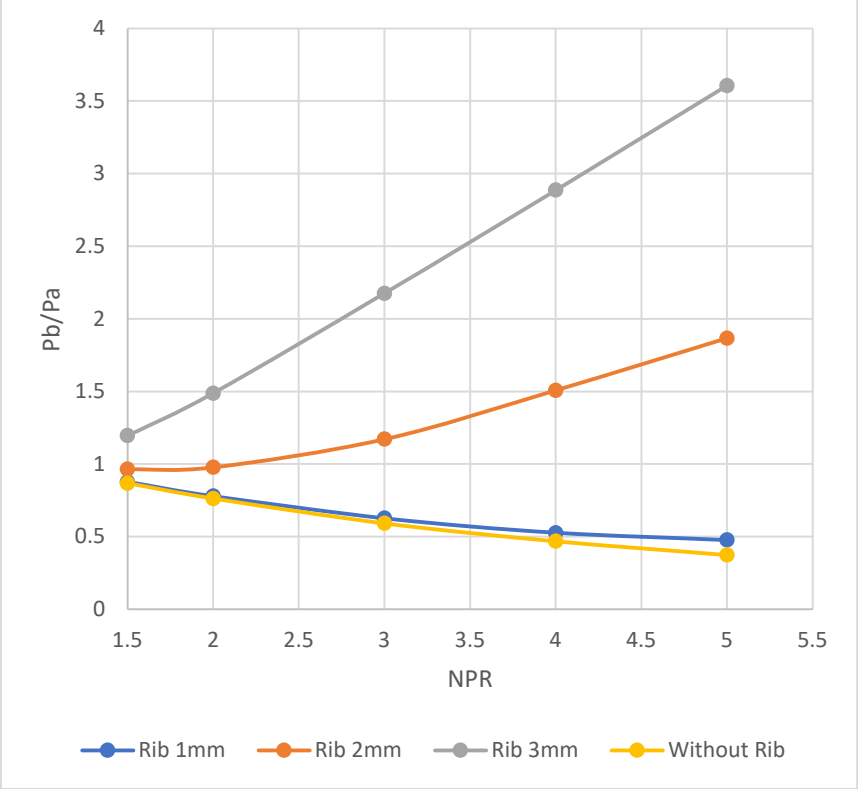

(c) L/D = 5

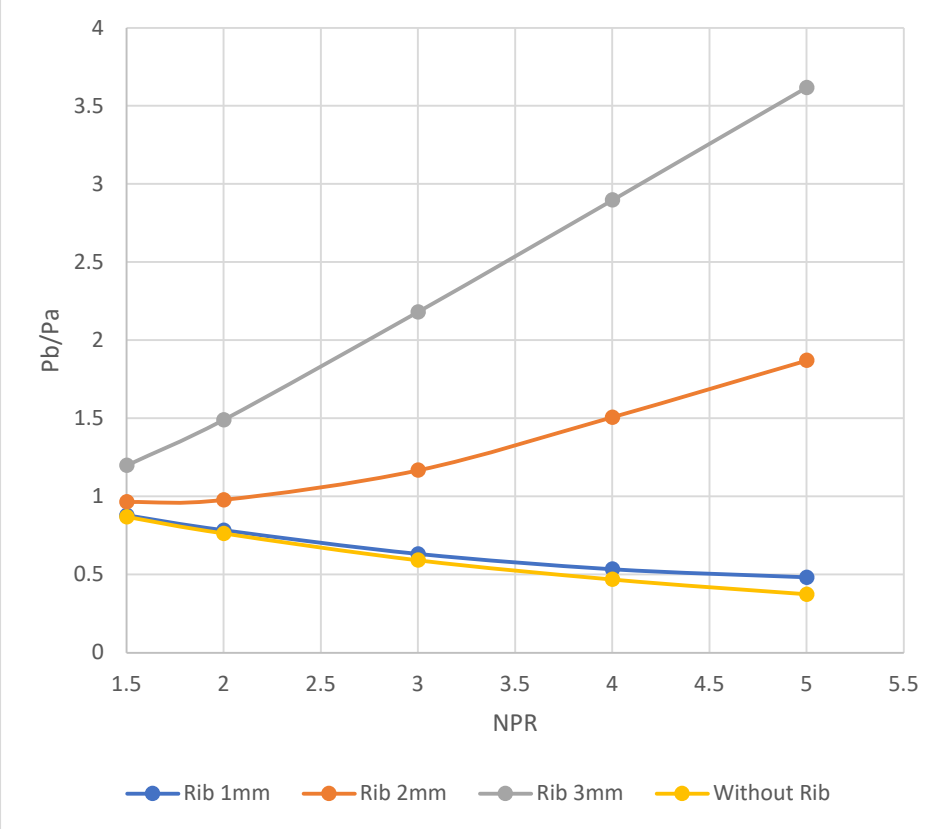

(d) L/D = 6

Fig. 10. Base Pressure Vs. NPR for numerous Duct segments

5.1.5 Base Pressure Results for Rib Location at L/D = 3.0

The rib location with L/D = 3 yields no valuable results, as shown in Figures 11(a) through (c). Hence, we have omitted the discussion about this location, as it does not result in a considerable rise in the base pressure, since our base pressure increase is achieved within the first three locations. Finally, the authors suggest that the rib located at L/D = 1 and 1.5 is the ideal location of the ribs for a duct of 22 mm diameter.

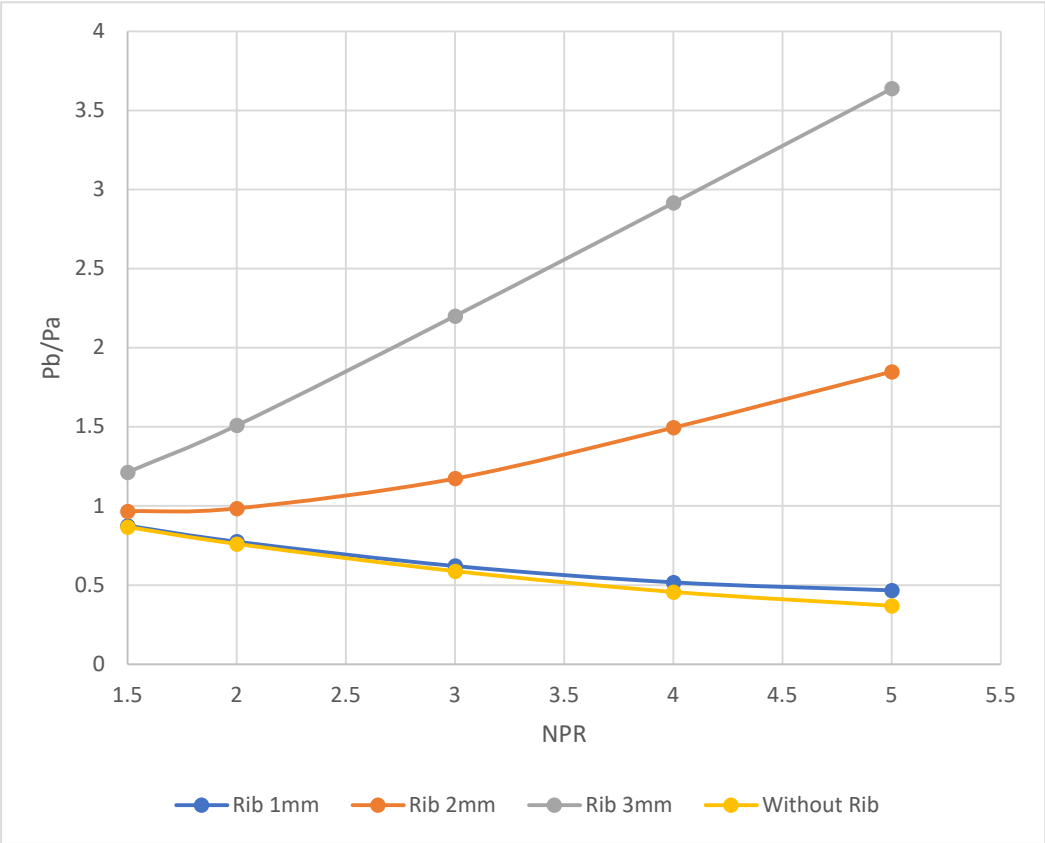

(a) L/D = 4

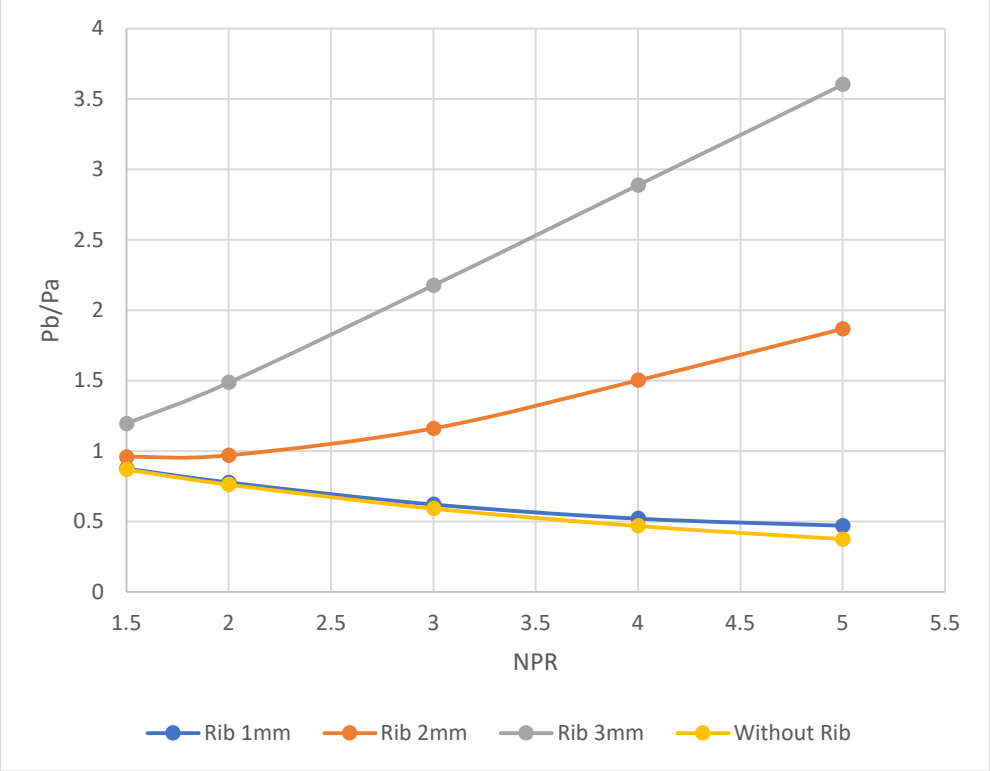

(b) L/D = 5

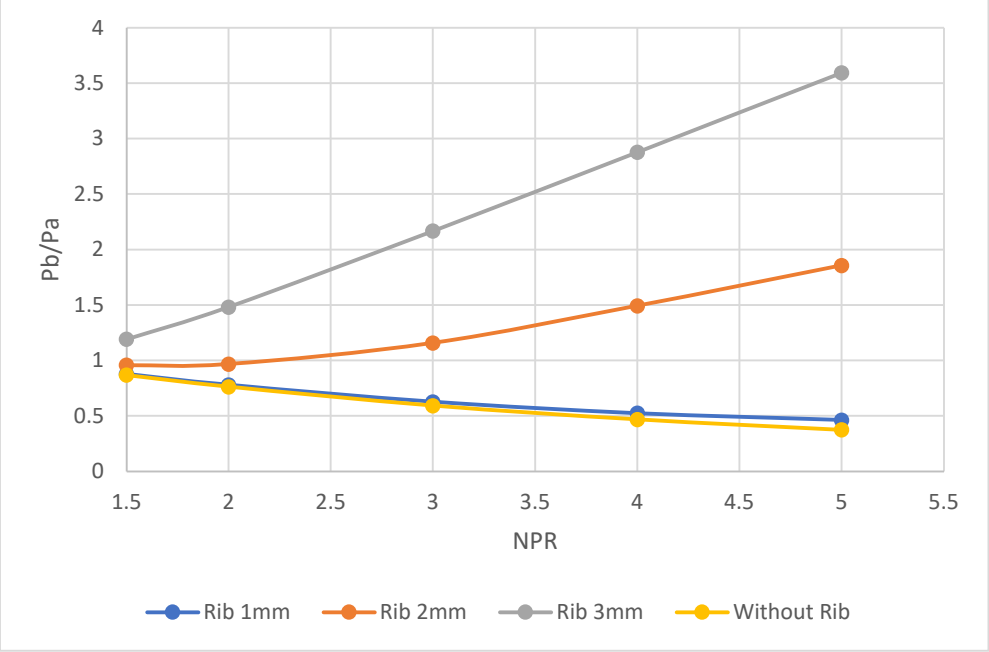

(c) L/D = 6

Fig. 11. Base Pressure Vs. NPR for numerous Duct segments

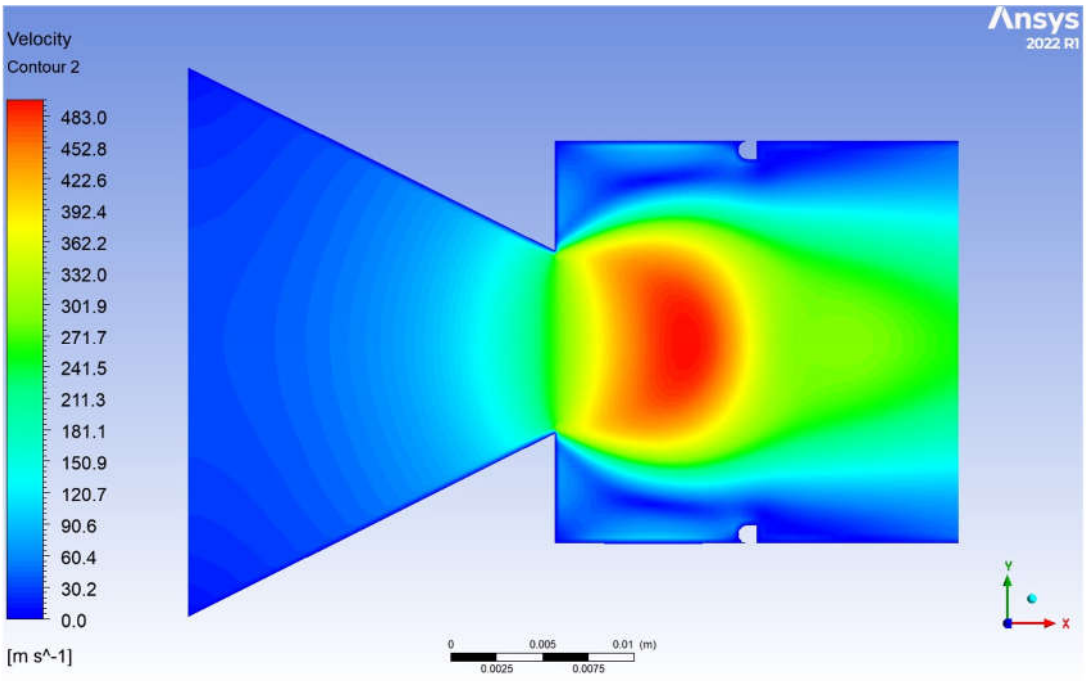

(a) Velocity Contour

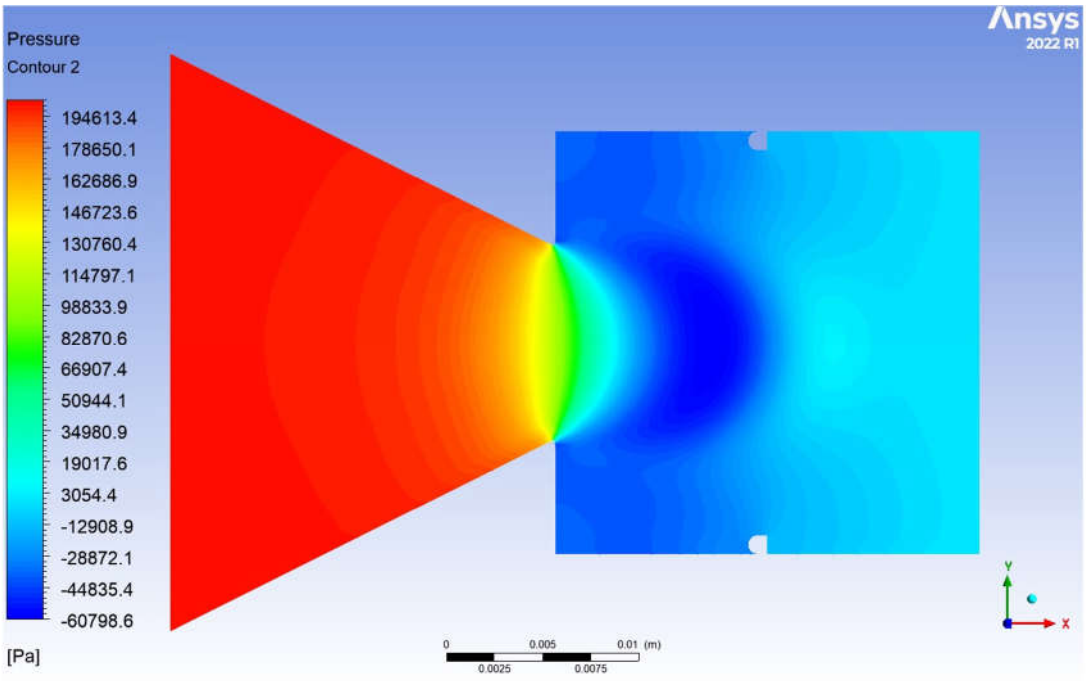

(b) Pressure Contour

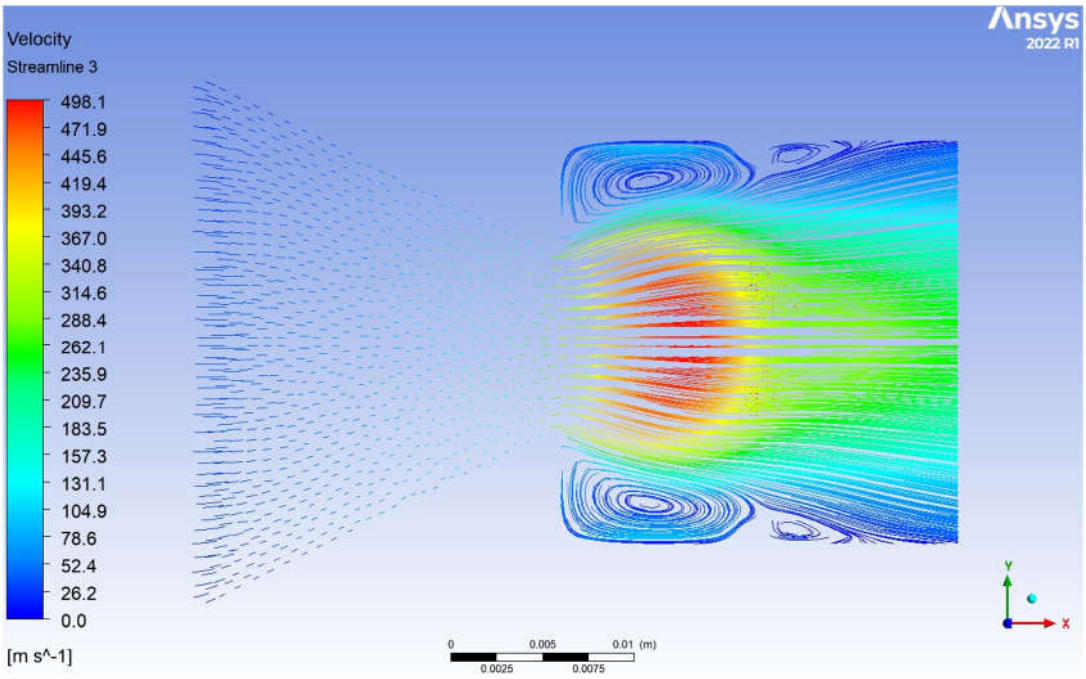

(c) Streamline Contour

Fig. 12 Velocity, Pressure, and Streamline Contour

Fig. 12 (a) to (c) shows the velocity, pressure, and streamline contours for rib location at L/D = 0.5. Fig. 12(a) shows the velocity contour, where the central jet has the highest velocity. However, due to the sudden increase in the area, the flow decelerates in the corner, and a reverse pattern is observed, as shown in Fig. 12(b), which displays the pressure contour. When we examine the streamline contour, it is evident that there are recirculation zones in the corner and near the rib.

6. Conclusions:

Based on the discussion above, we may conclude that the base pressure is a strong function of the nozzle pressure ratio and the rib locations. In this study, we have considered two orientations of the rib. For orientation one, the curved part of the D-shaped rib faces the exiting shear layer from the converging nozzle, and in orientation two, the straight part of the rib faces the shear layer. The results show that the base pressure values are slightly higher for orientation two than for rib orientation. This change is due to the sharp corner being upstream and downstream for other orientations.

For this duct diameter, the reattachment length seems to be around L/D = 1 to 1.5. That may be the main reason that when the rib is shifted to L/D = 2 and 3, it does not substantially increase the base pressure. As we know, this increase in the base pressure is due to the interaction of the waves, the location of the reattachment point, duct size, and the strength of the secondary vortices.

For rib location L/D = 0.5, the flow is in transition and has not been established; hence, the base pressure values are lower than the base pressure values for rib locations at L/D = 1 and 1.5.

There is a progressive rise in the base pressure values when the rib is located at L/D = 1, and then when the rib is located at L/D = 1.5, there is a marginal change in the base pressure values. With a further shift in the rib locations downstream (i.e., L/D = 2 and 3), there is no change in the base pressure values, as they have reached a steady state. Hence, one

suggestion is to analyze the results on a case-by-case basis. The reattachment length depends on the Mach number, duct diameter, expansion levels, and length-to-diameter ratio.

References

1. Khan, A., Rajendran, P., Sidhu, J.S.S., & Sharifpur, M. (2023). Experimental investigation of suddenly expanded flow at sonic and supersonic Mach numbers using semi-circular ribs: a comparative study between experimental, single-layer, deep neural network (SLNN and DNN) models. European Physical Journal Plus, 138(4), 314. https://doi.org/10.1140/epjp/s13360-023-03853-1
2. Khan, A., Mazlan, N.M., & Sulaeman, E. (2022). Effect of ribs as passive control on base pressure at sonic Mach numbers. CFD Letters, 14(1), 140–151. https://doi.org/10.37934/cfdl.14.1.140151
3. Khan, A., Khan, S.A., Raja, V., Aabid, A., & Baig, M. (2024). Effect of ribs in a suddenly expanded flow at sonic Mach number. Heliyon, 10(9), e30313. https://doi.org/10.1016/j.heliyon.2024.e30313
4. Khan, A., Mazlan, N.M., & Ismail, M.A. (2020). Numerical simulation of suddenly expanded flow from a converging nozzle at sonic Mach number. In Lecture Notes in Mechanical Engineering, pp. 349–359. https://doi.org/10.1007/978-981-15-4756-0_29
5. Khan, A., Akhtar, M.N., Aabid, A., Baig, M., & Khan, S.A. (2024). Comprehensive CFD analysis of base pressure control using quarter ribs in a sudden expansion duct at sonic Mach numbers. International Journal of Thermofluids, 24, 100908. https://doi.org/10.1016/j.ijft.2024.100908
6. Khan, A., Akhtar, M.N., Khan, S.A., Aabid, A., & Baig, M. (2024). Base pressure control with semi-circular ribs at the critical Mach number. Fluid Dynamics and Materials Processing, 20(9), 2007–2028. https://doi.org/10.32604/fdmp.2024.049368
7. Gao, S., & Liu, J. (2020). Adaptive neural network vibration control of a flexible aircraft wing system with input signal quantization. Aerospace Science and Technology, 96. https://doi.org/10.1016/j.ast.2019.105593
8. Li, S., Li, L., Huang, W., Zhao, Y., & Chen, J. (2020). Design and investigation of an equal cone-variable Mach number wave rider in hypersonic flow. Aerospace Science and Technology, 96. https://doi.org/10.1016/j.ast.2019.105540
9. Lu, J., Huang, J., & Lu, F. (2020). Kernel extreme learning machine with iterative picking scheme for failure diagnosis of a turbofan engine. Aerospace Science and Technology, 96. https://doi.org/10.1016/j.ast.2019.105539
10. Yan, C., Yin, Z., Shen, X., Mi, D., Guo, F., & Long, D. (2020). Surrogate-based optimization with improved support vector regression for non-circular vent hole on aero-engine turbine disk. Aerospace Science and Technology, 96. https://doi.org/10.1016/j.ast.2019.105332
11. Rathakrishnan, Ethirajan, Ramanaraju, O. V, & Padmanaban, K. (1989). Influence of Cavities on Suddenly Expanded Flow Field. Mechanics Research Communications, 16(3), 139-146.
12. Pandey, Krishna Murari, & Rathakrishnan, E. (2006). Influence of Cavities on Flow Development in Sudden Expansions. International Journal of Turbo and Jet Engines, 23(2), 97.
13. Pathan, K. A., Dabeer, P., & Khan, S. A. (2019). Effect of Nozzle Pressure Ratio and Control Jets Location to Control Base Pressure in Suddenly Expanded Flows. Journal of Applied Fluid Mechanics, 12(4), 1127-1135. https://doi.org/10.29252/jafm.12.04.29495
14. Vikramaditya, N., Viji & Verma, S. & Ali, Naveed & Thakur, D. (2017). Base Pressure Fluctuations on a Typical Missile Configuration in Presence of Base Cavity. Journal of Spacecraft and Rockets. 55. 1-11. 10.2514/1.A33926.
15. Khan, S. A., Asadullah, M., Ahmaed, F.G.M., Jalaluddeen, A., Baig, & MAA. (2018). Passive Control of Base Drag in Compressible Subsonic Flow Using Multiple Cavity. International Journal of Mechanical and Production Engineering Research and Development, 8(4), 39-44. https://doi.org/10.24247/ijmperdaug20185

16. Asadullah, M., Khan, S. A., Soudagar, M. E. M., & Vaishak, T. R. (2018). A Comparison of the Effect of Single and Multiple Cavities on Base Flows. In 2018, IEEE 5th International Conference on Engineering Technologies and Applied Sciences (ICETAS) (pp. 1-5). IEEE.
17. Rajendran, P., Sethuraman, V., & Khan, S. A. (2019). A Cost-Effective Data Acquisition Instrumentation for Measurement of Base Pressure and Wall Pressure in Suddenly Expanded Flow-Through Ducts. Journal of Advanced Research in Fluid Mechanics and Thermal Sciences, 60(1), 112-123.
18. Afzal, A., Aabid, A., Khan, A., Afghan, S., Rajak, U., Nath, T., & Kumar, R. (2020). Response surface analysis, clustering, and random forest regression of pressure in suddenly expanded high-speed aerodynamic flows. Aerospace Science and Technology, 107, 106318. https://doi.org/10.1016/j.ast.2020.106318
19. Afzal, A., Khan, S. A., Islam, T., Jilte, R. D., Khan, A., & Soudagar, M. E. M. (2020). Investigation and backpropagation modeling of base pressure at sonic and supersonic Mach numbers. Physics of Fluids, 32(July), 096109. https://doi.org/10.1063/5.0022015
20. Bashir, M., Rajendran, P., Khan, A., Raja, V., & Khan, S. A. (2023). Numerical investigation of turbulence models with emphasis on turbulent intensity at low Reynolds number flows. Advances in Aircraft and Spacecraft Science, 10(4), 303-315. https://doi.org/10.12989/aas.2023.10.4.303
21. Baig, M.A.A., Khan, S. A., Al-Mufadi, F., & Rathakrishnan, E. (2011). Control of base flows with microjets. International Journal of Turbo and Jet Engines, 28(1), 59-69. DOI:10.1515/tjj. 2011.009
22. Rehman, S., & Khan, S. A. (2008). Control of base pressure with micro-jets: Part I. Aircraft Engineering and Aerospace Technology, 80(2), 158-164. https://doi.org/10.1108/00022660810859373
23. Faheem, M., Afghan Khan, S., Asrar, W., Khan, A., & Kumar, R. (2021). Experimental study on the mean flow characteristics of a supersonic multiple jet configuration. Aerospace Science and Technology, 108, 106377. DOI:10.1016/j.ast.2020.106377
24. Sajali, M.F.M., Aabid, A., Khan, S.A., Sulaeman, E., & Mehaboobali, F.A.G. (2019). Numerical investigation of the flow field of a non-circular cylinder. CFD Letters, 11(5), 37-49. https://www.akademiabaru.com/submit/index.php/cfdl/article/view/3161
25. Khan, S.A., Asadullah, M., Fharukh Ahmed, G.M., Jalaluddeen, A., & Ali Baig, M.A. (2018). Passive control of base drag in compressible subsonic flow using multiple cavities. International Journal of Mechanical and Production Engineering Research and Development, 8(4), 39-44. DOI:10.24247/ijmperdaug20185
26. E Rathakrishnan. (2001). Effect of ribs on suddenly expanded flows. AIAA Journal 39(7), 1402-1404. https://doi.org/10.2514/2.1461.